Pressure drawdown well tests in fractured porous media

I. I. Bogdanov, V. V. Mourzenko, J. -F. Thovert, P. M. Adler

▶ To cite this version:

I. I. Bogdanov, V. V. Mourzenko, J. -F. Thovert, P. M. Adler. Pressure drawdown well tests in fractured porous media. Water Resources Research, 2003, 39, p. 289-310. 10.1029/2000WR000080 . insu-03598430

HAL Id: insu-03598430

https://hal-insu.archives-ouvertes.fr/insu-03598430

Submitted on 5 Mar 2022

Pressure drawdown well tests in fractured porous media

I. I. Bogdanov

Laboratoire de Combustion et de Detonique, Chasseneuil, France

Institut de Physique du Globe de Paris, Paris, France

V. V. Mourzenko and J.-F. Thovert

Laboratoire de Combustion et de Detonique, Chasseneuil, France

P. M. Adler

Institut de Physique du Globe de Paris, Paris, France

[1]   A general three-dimensional numerical model for single-phase, slightly compressible flow through fractured porous media is introduced. It is based on a discrete fracture representation. Applications to the simulation of pressure drawdown well tests are presented, for complex situations where the well intercepts a random fracture network with various fracture densities and conductivities. The well pressure response can be modeled as a function of its interconnectivity with the fracture network.   *INDEX TERMS:* 1829 Hydrology: Groundwater hydrology; 3210 Mathematical Geophysics: Modeling; 3230 Mathematical Geophysics: Numerical solutions; 5104 Physical Properties of Rocks: Fracture and flow; 5114 Physical Properties of Rocks: Permeability and porosity; *KEYWORDS:* well test, fractured medium, compressible flow, pressure drawdown, reservoir

1. Introduction

[2] This work addresses single-phase, slightly compressible flow through fractured porous media. A very general three-dimensional numerical model based on a discrete fracture representation is proposed, together with an application to the simulation of pressure drawdown well testing, which is an established and widely used technique for the evaluation of formation transport properties. It consists in measuring the pressure response to flow from a well, generally under nonstationary conditions.

[3] Owing to the specific transport properties of fractures, the flow through a naturally fractured porous medium differs drastically from that in a conventional porous medium formed by intergranular porosity. The key feature is that the porous matrix provides the main storage for the fluids, while transport takes place mainly through the fracture system. Furthermore, matrix/fracture flow interactions govern many of the medium transport properties. Because of the complexity and diversity of most natural fracture systems, the determination of fractured porous media transport properties remains an open issue of great practical importance. For instance, the present numerical tool can be applied for the interpretation of well test data, in order to quantify the characteristics of a reservoir or, conversely, to optimize the design of a producing well, given the reservoir characteristics.

[4] The numerous existing models of transient, slightly compressible flow through fractured porous media are actually based on few different approaches. Since the early 1960s, when it was first proposed by *Barenblatt and Zheltov* [1960], the model based on the concept of two overlapping continua underlies the theory of flow through double-porosity media. The model has been used extensively for decades starting from the generalization proposed by *Warren and Root* [1963] with media consisting of rectangular porous parallelepipeds. Many analytical treatments in the framework of this model have been presented in the review article by *Chen* [1989]. Recently, *Reis* [1998] and *Gwo et al.* [1998] allowed for a larger degree of randomness, by incorporating in the model field observations of fracture spacing distribution.

[5] The discrete approach allows a more detailed description of the matrix/fracture flow interaction accounting for the flow behavior in individual elements of the medium. It has been applied successfully for a variety of regular finite or infinite fracture systems [see, e.g., *Snow*, 1969; *Wilson and Witherspoon*, 1974; *Boulton and Streltsova*, 1977a; *Young*, 1992; *Shikaze et al.*, 1998].

[6] In contrast with the previous analytical or finite difference numerical approaches, *Noetinger and Estebenet* [2000] describe a continuous-time random walk method to model transient flow in fractured rocks, and use it to determine the exchange coefficient involved in a dual-porosity formulation. Applications are restricted to small two-dimensional (2-D) regular test cases, but the approach should be applicable to more complex networks.

[7] An interesting approach for very dense fracture systems originated from the analysis of the multiple length scales in natural fracture networks and was motivated by the analogy with diffusion on fractals. *Acuna and Yortsos*

[1995] proposed such a model and numerically investigated the pressure transient response of finite fractals. *Mo et al.* [1998] describe a fracture network flow model based on algebraic topology, and analyze their results in relation to percolation theory. However, in both works, the matrix is impermeable and flow is restricted to the fracture network.

[8] Direct numerical determination of the permeability of fractured porous media was addressed by *Koudina et al.* [1998] and *Bogdanov et al.* [2002]. Their numerical model makes use of a full 3-D description of the discrete fracture system, and the steady single-phase flow equations are solved in periodic porous unit cells containing arbitrary random fracture networks. Integration of the local flow field yields the macroscopic permeability.

[9] We present in this paper an extension to unsteady compressible flow of the numerical models of *Koudina et al.* [1998] and *Bogdanov et al.* [2002], and applications to the simulation of pressure drawdown well tests in various model situations.

[10] This paper is organized as follows. The governing equations are presented in section 2 for the flow in the rock matrix, in the fractures, and in the well and for their coupling. A list of the symbols and notations is provided in Table 1.

[11] Then the numerical model is described in section 3. This includes first the construction of an unstructured three-dimensional mesh of the fractured medium, where discrete fractures are represented by surface elements. The well is introduced in a second step and does not have to coincide with edges of the mesh. The partial differential equations are discretized in a finite volume fully implicit formulation, with particular care taken about the description of the exchanges between the well and its surroundings.

[12] In section 4, a few classical analytical solutions for wells in unfractured media are recalled and used to assess the performances of the numerical model.

[13] Analytical results for a well intersecting a single fracture are reviewed in section 5.

[14] Finally, randomly fractured media are addressed in section 6. Examples of pressure drawdown curves are presented first. They give rise to a variety of behaviors, which are discussed in comparison with the case of the well intersecting a single fracture. Then wells at various locations in media with various fracture density and conductivity are considered. The well pressure response is shown to depend on its interconnectivity with the fracture network. For long times, it can be modeled as a well in a homogeneous medium with an apparent radius, which is generally larger than its real radius and depends on the density of well/fracture intersections.

[15] Some concluding remarks are given in section 7.

2. Governing Equations

[16] The fractured porous medium can be represented as an arbitrary, generally random, set of fractures embedded into a solid porous matrix whose physical properties may vary with space. The fractures may intersect or not. They also interact by means of flow through the adjacent volumes of porous matrix. Hence pressure is continuous throughout the medium.

[17] However, at the large scale, each fracture can be viewed as vanishingly thin, with transport properties that generally differ drastically from those of the ambient porous matrix, and may be considered as a surface of singularity. For instance, a steep pressure gradient may exist across a poorly conducting fracture, which results in an apparent pressure jump at the macroscopic scale. Similarly, the flow rates normal to the two surfaces of a very conducting fracture may differ significantly. In addition, the typical time for pressure variations in transient flows is quite different in the matrix and in the fractures.

[18] The discrete fracture model used in the present work explicitly accounts for these features. Therefore it allows detailed investigations of transitory flow regimes and of the influence of the well intersections with the fracture network.

2.1. Flow in the Porous Matrix

[19] Consider a porous matrix with a bulk permeability K_m $[L^2]$ which may vary with space. Darcy law can be written for the local seepage velocity v in the matrix

$$v = -\frac{K_m}{\mu}\nabla P, \tag{1}$$

where μ is the fluid viscosity and P is the pressure. The continuity equation for slightly compressible flow reads as follows:

$$\epsilon_m C_m \frac{\partial P}{\partial t} + \nabla \cdot v = \delta_w J_w \tag{2}$$

where ϵ_m and C_m are the matrix porosity and total compressibility, respectively. The source term J_w on the right-hand side of equation (2) represents the exchanges with the well. The Dirac function δ_w has dimensions $[L^{-2}]$ (length of well per volume) and J_w has dimensions $[L^2 T^{-1}]$ (flow rate per unit length of well). On the scale of description used here, the well appears as a line without thickness.

[20] If the volumetric capacity $\epsilon_m C_m$ is constant, equation (2) can be written as

$$\frac{\partial P}{\partial t} - \nabla \cdot (D_m \nabla P) = \frac{\delta_w J_w}{\epsilon_m C_m}, \qquad D_m = \frac{K_m}{\mu \epsilon_m C_m} \tag{3}$$

where D_m is the matrix pressure diffusivity.

2.2. Flow in Fractures

[21] We assume that the hydraulic properties of a fracture can be characterized by two effective coefficients, namely, a conductivity σ $[L^3]$ and a cross-resistance ω $[L^{-1}]$ [see *Bogdanov et al.*, 2002]. The first coefficient relates the flow rate j per unit width of the fracture to the surface pressure gradient $\nabla_s P$ by the two-dimensional Darcy's law

$$j = -\frac{\sigma}{\mu}\nabla_s P \tag{4a}$$

where ∇_s is the gradient operator restricted to a surface, $\nabla_s = (I - nn) \cdot \nabla$. Here I is the unit tensor and n is the normal vector to the fracture plane. The second coefficient relates the pressure drop ΔP across a fracture to the normal seepage velocity $v_\perp$

$$v_\perp = -\frac{1}{\mu \omega}\Delta P. \tag{4b}$$

[22] For illustration, the fracture can be viewed as a plane channel of aperture b, filled with a porous material with permeability K_f, porosity ϵ_f, and total compressibility C_f. Then σ and ω are given by

$$\sigma = bK_f \quad , \quad \omega = \frac{b}{K_f} \tag{5}$$

A nonzero resistance ω may exist even for totally open channels, if their walls are partially clogged by a deposited chemical. *Onur and Satman* [1998] examined the influence of such a fracture skin on the well pressure response, in the framework of a double-porosity description.

[23] The continuity equation for the flow through a fracture reads as

$$b\,\epsilon_f\,C_f\frac{\partial P}{\partial t} + \nabla_s \cdot \boldsymbol{j} = (\boldsymbol{v}^- - \boldsymbol{v}^+) \cdot \boldsymbol{n} + b\delta_w J_w \tag{6}$$

where $\boldsymbol{v}^+$ is the seepage velocity in the matrix on the side of $\boldsymbol{n}$ and $\boldsymbol{v}^-$ is the seepage velocity on the opposite side. These velocities are given by equation (1). Again, if $b\epsilon_f C_f$ is constant in a fracture, a pressure diffusivity D_f can be defined, and equation (6) can be written as

$$\frac{\partial P}{\partial t} - \nabla_s \cdot \left(D_f \nabla_s P\right) = \frac{(\boldsymbol{v}^- - \boldsymbol{v}^+) \cdot \boldsymbol{n}}{b\epsilon_f C_f} + \frac{\delta_w J_w}{\epsilon_f C_f}, \qquad D_f = \frac{\sigma}{b\mu\epsilon_f C_f} \tag{7}$$

[24] The intersection line $\mathcal{I}_{ij}$ of two fractures S_i and S_j is supposed to have no specific contribution to the flow; thus the flow rates from $\mathcal{I}_{ij}$ to the adjacent fractures sum up to zero. Let $\boldsymbol{\nu}_{ij}$ and $\boldsymbol{\nu}_{ji}$ be two vectors perpendicular to the intersection $\mathcal{I}_{ij}$ which lie in the two fractures S_i and S_j, respectively. Then

$$\boldsymbol{\nu}_{ij} \cdot \left(\boldsymbol{j}_i^+ - \boldsymbol{j}_i^-\right) + \boldsymbol{\nu}_{ji} \cdot \left(\boldsymbol{j}_j^+ - \boldsymbol{j}_j^-\right) = 0 \tag{8}$$

where $\boldsymbol{j}_i^+$ (resp. $\boldsymbol{j}_i^-$) is the flux in S_i on the side of (resp. opposite to) $\boldsymbol{\nu}_{ij}$.

[25] Note that the simplifying assumptions of uniform $\epsilon_m C_m$ and $b\epsilon_f C_f$ used to write down the diffusion equations (3) and (7) and for the simulations in the present work are by no means a requirement for the numerical model, since the discretized equations are really based on the general equations (2) and (6).

2.3. Flow in the Well

[26] We assume that the flow within the well is laminar and quasi-steady. The latter assumption implies that storage effects in the well casing are negligible over a time step. Thus we obtain the following one-dimensional balance equation for a quasi-steady flow along the well axis [see, e.g., *Sudicky et al.*, 1995]

$$\frac{K_w}{\mu}\frac{\partial^2 P_w}{\partial s^2} - J_w(s) + Q_w\delta(s - s_h) = 0 \tag{9}$$

where P_w is the well pressure, s is the distance along the well from its head at s_h, Q_w is the total pumping rate applied

at the well head, and δ is the Dirac function. The well hydraulic conductivity K_w $[L^4]$ can be evaluated from the Hagen-Poiseuille equation for flow in a circular pipe,

$$K_w = \frac{\pi r_w^4}{8} \tag{10}$$

where r_w is the well radius. Since $r_w^2 \gg K_m$ and $r_w \gg b$, the well is highly conductive with respect to both the matrix rock and fractures. When pressure variations along the well are neglected, equation (9) reduces to

$$P_w(s) = P_{s_h} \tag{11}$$

2.4. Overall Boundary Conditions

[27] Standard boundary conditions in reservoir engineering are either of Dirichlet type, with an imposed far-field pressure P_∞, or of Neumann type, with no-flux conditions at the boundaries of a closed reservoir. Both types of conditions can be applied in the present model. However, since the investigated domain is necessarily finite in numerical simulations, these conditions have to be applied on the boundaries $\partial\tau$ of a finite domain τ,

$$P = P_\infty, \qquad \text{on } \partial\tau \tag{12a}$$

or

$$\boldsymbol{v} \cdot \boldsymbol{n}_\tau = 0, \qquad \boldsymbol{j} \cdot \boldsymbol{n}_\tau = 0, \qquad \text{on } \partial\tau \tag{12b}$$

where $\boldsymbol{n}_\tau$ is the unit vector normal to $\partial\tau$.

[28] In practice, a parallelepipedic cell τ was used in all the simulations. The well was always set along a straight line parallel to the z-axis, throughout the cell, and spatial periodicity was applied in the x-, y- and z-directions for the system geometry and for the pressure and flow fields. Hence this situation corresponds to a periodic square array of infinite vertical wells. Because of periodicity, no-flux surfaces exist in the three directions, which correspond to the cell boundaries $\partial\tau$; this no-flux condition is exact for simple axisymmetric cases and only approximate for more complex cases such as randomly fractured media. Two successive horizontal no-flux surfaces can be regarded as the bottom and ceiling of a producing layer between impervious barriers. Similarly, the vertical no-flux surfaces can be interpreted as the lateral boundaries of a closed reservoir.

[29] Of course, given the characteristics of an actual reservoir, this periodicity condition can be straightforwardly replaced by conditions (12) on an arbitrary surface $\partial\tau$.

[30] All the simulations reported here correspond to a pressure drawdown test, i.e., to a well producing at constant rate Q_w from a field initially at rest

$$P(\boldsymbol{r}, t = 0) = P_0 \tag{13}$$

The initial pressure P_0 is arbitrary and can be taken as $P_0 = 0$ without loss of generality. Q_w corresponds here to the flow rate from the portion of the well contained in a single cell of the periodic medium. If the pressure variations along the well are taken into account, the imposed flux Q_w is built in

the conservation equation (9). If the simplified equation (11) is applied, P_{sh} has to be determined from the condition

$$\int_{well\cap\tau} J_w(s)\mathrm{d}s = Q_w \qquad (14)$$

2.5. Dimensionless Formulation

[31] Dimensionless variables, denoted by primes, can be introduced by using characteristic quantities of the problem. A possible choice, based on the system properties b, R, K_m, μ, and D_m and on a typical pumping rate Q, is

$$\boldsymbol{r} = R\boldsymbol{r}', \qquad t = \frac{R^2}{D_m}t', \qquad P = \frac{\mu Q}{RK_m}P' \qquad (15a)$$

$$\boldsymbol{v} = \frac{Q}{R^2}\boldsymbol{v}', \qquad \boldsymbol{j} = \frac{Q}{R}\boldsymbol{j}', \qquad J_w = \frac{Q}{R}J_w' \qquad (15b)$$

$$K_w = R^2 K_m K_w', \qquad Q_w = Q\,Q_w', \qquad (15c)$$

$$\sigma = R\,K_m\sigma', \qquad \omega = \frac{R}{K_m}\omega', \qquad \eta = \frac{\epsilon_f C_f b}{\epsilon_m C_m R} \qquad (15d)$$

The unit scale R is a characteristic lateral extent of the fractures; for instance, it can be the radius of the circle into which the fracture is inscribed; $\boldsymbol{r}$ is the vector which denotes the position with respect to a fixed reference frame.

[32] Other choices are possible. In particular, the well radius r_w can be used as the characteristic length scale instead of the fracture size R. This is appropriate to describe the very early stage of a well test, when the flow is confined very near to the well [*Earlougher*, 1977]. This length scale is not used in this paper. Alternatively, the size of the drainage area A of a closed reservoir can be used as length unit, as done in section 4 (see equation (37)).

[33] As an illustration of the definition (15), for an oil with viscosity 10^{-2} Pa s, compressibility 0.3×10^{-8} Pa^{-1}, a porosity $\epsilon_m = 0.1$ and a permeability K_m ranging from 1 mD to 1 D, D_m ranges from 3×10^{-4} to 0.3 m^2 s^{-1}, and the timescale R^2/D_m from 5 minutes to 3 days for $R = 10$ m and from 10 hours to 1 year, for $R = 100$ m.

[34] Note that all the dimensionless quantities are denoted by a prime, and they are implicitly defined by equation (15). For instance, the aperture b, with the dimension of a length, is made dimensionless by R

$$b' = \frac{b}{R} \qquad (16)$$

and the same is done for other quantities.

[35] With the definitions (15), the complete set of governing equations then reads in the matrix,

$$\boldsymbol{v}' = -\nabla'P', \quad \frac{\partial P'}{\partial t'} - \nabla'^2 P' = \delta_w' J_w' \qquad (17a)$$

in the fractures,

$$\boldsymbol{j}' = -\sigma'\nabla_s'P', \qquad \boldsymbol{v}_\perp' = -\frac{1}{\omega'}\Delta P',$$

$$\frac{\partial P'}{\partial t'} - \frac{\sigma'}{\eta}\nabla'^2 P' = \frac{(\boldsymbol{v}'^- - \boldsymbol{v}'^+)\cdot\boldsymbol{n}}{\eta} + \frac{b'}{\eta}\delta_w' J_w' \qquad (17b)$$

and in the well

$$K_w'\frac{\partial^2 P_w'}{\partial s'^2} - J_w'(s) + Q_w'\delta'(s' - s_h') = 0 \qquad (17c)$$

Equations (17b) and (17c) show that the problem is governed by five dimensionless numbers, relative to the fracture (b', σ', ω', η) and well (K_w') properties.

[36] In the present work, we only consider very conducting fractures and neglect pressure variations along the well. Unless otherwise stated, all the results are given for $\omega' \to 0$, $K_w' \to \infty$, $b' = \eta = 10^{-3}$, and $\sigma' \gg 1$.

3. Numerical Model

[37] We will consider in the present work both simple deterministic test configurations and more realistic and complex randomly fractured porous media. Whereas specific discretization techniques could be used in the first situations, for instance, with local grid refinements [see, e.g., *Banerjee et al.*, 2000], we are really interested in the latter case where geometrical randomness requires great flexibility.

[38] The numerical model is a generalization of what has been done for flow in fracture networks by *Koudina et al.* [1998] and for flow in fractured porous media by *Bogdanov et al.* [2002].

[39] The simulations consist of two steps. The first step is to discretize the system geometry, i.e., the fracture network, the porous medium surrounding the fractures, and the well, in a consistent way. The second step is to discretize the partial differential equations (2), (6), and (9), in a finite volume, time-implicit formulation.

3.1. Triangulation of Fractured Media and Description of the Well Geometry

[40] In order to pave the whole space with tetrahedra, the fracture network is triangulated first as described by *Koudina et al.* [1998], by an advancing front technique, starting from the fracture contours and intersection lines. Then the space located in between the fractures is also paved by an advancing front technique, as described by *Bogdanov et al.* [2002]. The fractures provide the boundary surface enclosing the 3-D domain to be covered by the mesh, i.e., the initial front of the generation process. The basic step consists of adding a fourth point to the existing triangles in order to build a tetrahedron; hence the space is progressively covered by tetrahedra. The scale of the discretization is controlled by a typical spacing δ_M between the mesh points. Actually, this technique is much more involved than it may seem at first sight; the position of the fourth point has to be carefully checked so that the additional tetrahedron does not overlap with previous elementary volumes and so that it does not cross any fracture.

[41] A 3-D view of an example of a triangulated fractured medium is displayed in Figure 1a. The fractures are hexagons which are inscribed in circles of radius R. The cell size is $L = 4R$; the cell contains $N_{fr} = 32$ fractures. The triangulation with $\delta_M = R/4$ contains 4575 node points, 56748 triangles, and 28,374 tetrahedra. The discretization of the fractures is also displayed in this figure. The samples used in section 6 are actually larger than this
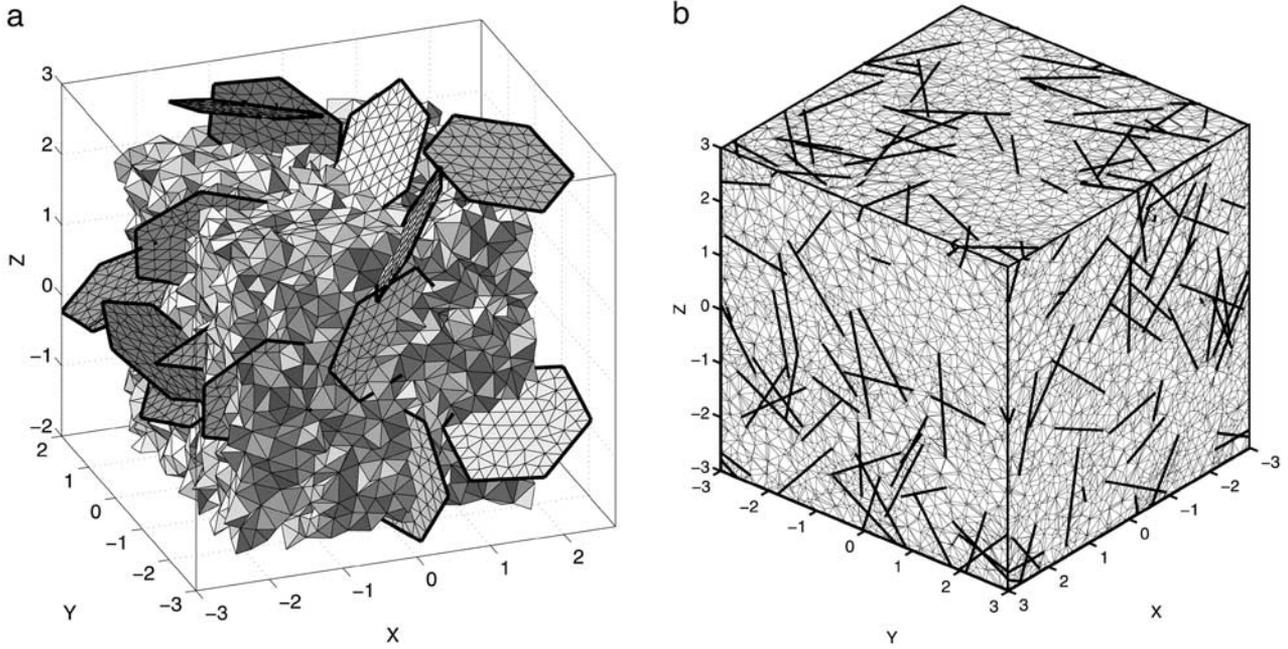
Figure 1. Three-dimensional views of triangulated periodic fractured media. The illustrative example in Figure 1a contains N_{fr}=32 hexagonal fractures with circumscribed radius R. The cell size is $L = 4R$, and $\delta_M = R/4$. For the sake of clarity, the edges of the fractures have been thickened. The tetrahedral volume elements with their centers in the cubic unit cell $-2\,R \leq x, y, z \leq +2\,R$ are displayed. The protruding fractures sit astride the boundaries with the neighboring cells. The sample in Figure 1b is one of those used in section 6, with $L = 6R$, $N_{fr} = 166$, and $\delta_M = R/4$. The intersections of the fractures (thick lines) and of the tetrahedral volume elements with the cell boundaries are shown.

example, with $L = 6R$ (see Figure 1b); they typically contain 2×10^4 nodes, 2×10^5 triangles, and 10^5 tetrahedra.

[42] In a subsequent step, the well is superimposed on the 3-D unstructured mesh, as described in section 3.2.3. For any given well geometry, the intersections of the well with the triangles of the numerical mesh are determined. This yields on one hand the locations of the intersections of the well with fractures and, on the other hand, the end points of the well segments contained in the matrix tetrahedral volume elements.

[43] Note that the initial triangulation is performed without considering the well. A possible alternative is to take the well into account from the start during the construction of the mesh, so that mesh points would be distributed with arbitrary spacing right on the well. However, the 3-D triangulation of complex media is a time-consuming step. The present procedure allows one to perform it only once for a given medium, and then to vary the well geometry or location at negligible cost.

[44] The typical size δ_M of the volume and surface elements has to be set small in comparison with the typical size R of the fractures, for a good rendering of the fractured medium geometry, and large in comparison with the well radius r_w, since the well is considered as a line without thickness in the numerical model. Recall also that r_w is supposed to be large in comparison with the fracture aperture. Finally, in the present simulations, we only consider highly conducting fractures, which implies

that b^2 is large in comparison with K_m. This hierarchy of scales can be summarized as

$$\sqrt{K_m} \ll b \ll r_w \ll \delta_M \ll R \qquad (18)$$

3.2. Finite Volume Formulation

[45] When the triangulation step is completed, the rock matrix is represented by tetrahedral volume elements, with given properties ϵ_m, C_m, and K_m, and the fractures by triangular surface elements with given properties ϵ_f, C_f, b, σ, and ω. All these parameters can be set independently, on a per-element basis. The pressure is evaluated at the vertices of the surface and volume elements (open circles in Figure 2c). The well is represented by a series of segments in the volume elements that it crosses. The pressure in the well is evaluated at the midpoints of these segments and at the intersection of the well with fractures (black dots in Figure 2c).

[46] However, according to equation (4b), pressure may take different values in the matrix on either sides of a fracture. It is therefore necessary to solve for these two values $P^{\pm}$ of the pressure (see Figure 2b). A third value of the pressure P_f is introduced, in the middle plane of the fracture, which is used for equation (6) in the fracture. More complex situations occur along the intersection line of two fractures (with 5 values of P) and at the intersection point of three fractures (with 9 values of P).
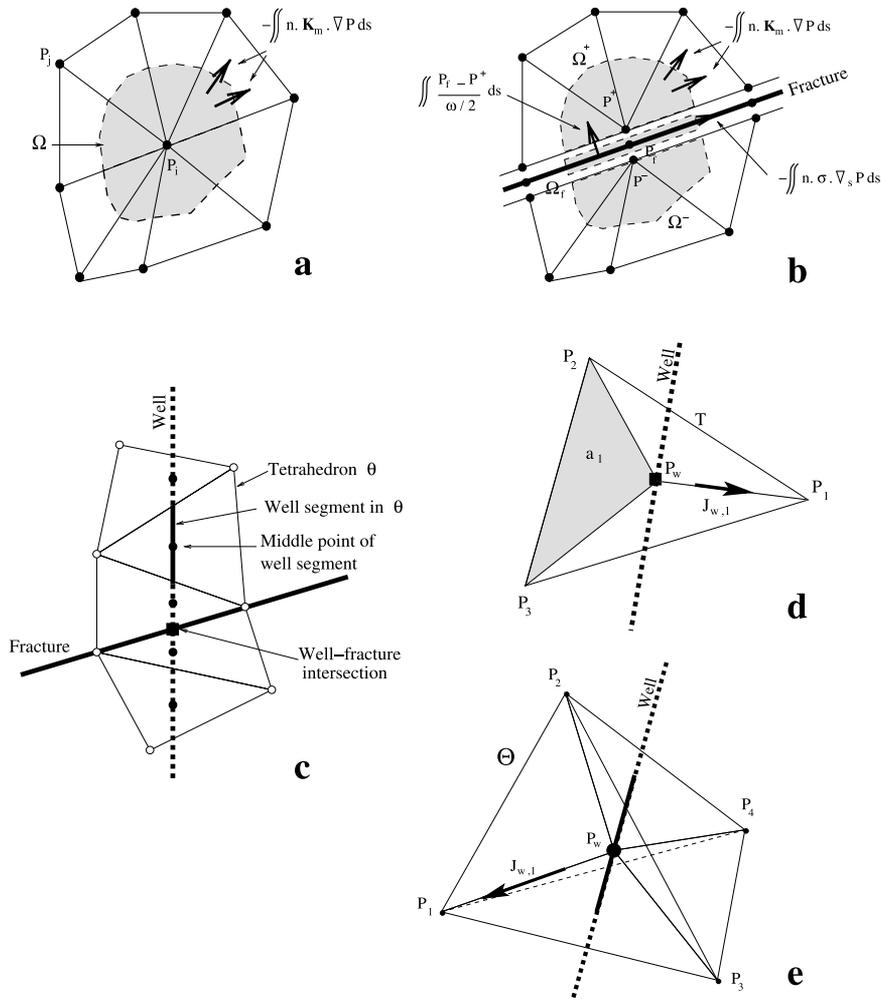
Figure 2. Control volumes around a point in the matrix (a) and on a fracture (b). Two-dimensional illustration of the introduction of the well in the mesh (c). Well intersection with a fracture surface element (d), and with a matrix volume element (e).

[47] The equations for the node pressures are obtained by integration of the balance equations (2), (6), and (9) over a control volume Ω around each mesh point.

[48] Several types of control volumes exist, according to the location of the mesh point, in the bulk of the rock matrix or on a fracture, with or without a well nearby. These different situations are considered below.

3.2.1. Control Volume in the Rock Matrix

[49] Let us start with the simplest case of a node point in the bulk of the matrix, without a well nearby. This situation is depicted in Figure 2a. The control volume Ω is made up of one fourth of all the tetrahedral volume elements incident to the point under consideration. The continuity equation (2) is integrated over the volume Ω, with application of the divergence theorem to convert the flux divergence into a surface integral

$$\int_\Omega \left(\epsilon_m C_m \frac{\partial P}{\partial t} + \nabla \cdot \boldsymbol{v} \right) \mathrm{d}v = \int_\Omega \epsilon_m C_m \frac{\partial P}{\partial t} \mathrm{d}v + \int_{\partial\Omega} \boldsymbol{n} \cdot \boldsymbol{v} \, \mathrm{d}s = 0$$

(19)

Recall that the matrix properties ϵ_m, C_m, and K_m are taken as uniform over each tetrahedral volume element. The seepage velocity $\boldsymbol{v}$ in each tetrahedron is evaluated from equation (1),

where the pressure gradient is deduced from the pressures at the four vertices. Thus $\boldsymbol{v}$ is piecewise constant over $\partial\Omega$, and it is a linear combination of the pressure at the center point and at the neighboring mesh points. Therefore, after cumbersome but straightforward calculations, the balance equation (19) can finally be written as a linear equation relating the pressures P_i at point i and P_j at surrounding points

$$C_i \frac{\partial P_i}{\partial t} = \sum_j M_{ij} \left(P_j - P_i \right)$$

(20)

where the summation is taken over all neighbors j. C_i is the volume integral of $\epsilon_m C_m$ over Ω_i. The matrix of coefficients M_{ij} depends on the geometry of the control volume and on the permeabilities K_m of the volume elements it intercepts. It is symmetric, since the fluid exchange between the control volumes Ω_i and Ω_j around the points i and j is evaluated in the same way when equation (19) is applied to Ω_i and Ω_j, which ensures global mass conservation.

3.2.2. Mesh Point on a Fracture

[50] As already mentioned, three pressures $P^\pm$ and P_f are defined for a mesh point on a fracture F. To obtain the necessary equations, three balance equations are written,

over the three control volumes depicted in Figure 2b, $\Omega^{\pm}$ on either side of the fracture and Ω_f in the fracture.

[51] The volumes $\Omega^{\pm}$ are treated as in the previous case, with an exchange term $q^{\pm}$ with the fracture added to equation (19)

$$\int_{\Omega^{\pm}} \epsilon_m C_m \frac{\partial P^{\pm}}{\partial t} dv + \int_{\partial\Omega^{\pm}-F} \mathbf{n} \cdot \mathbf{v} \, ds = q^{\pm} \qquad (21a)$$

Ω_f is made of one third of each triangular surface elements adjacent to the point under consideration. Equation (6) is integrated over Ω_f, which yields

$$\int_{\Omega_f} b\epsilon_f C_f \frac{\partial P_f}{\partial t} ds + \int_{\partial\Omega_f} \mathbf{n} \cdot \mathbf{j} \, dl = q^- - q^+ \qquad (21b)$$

The flux $\mathbf{j}$ in each triangle intercepting Ω_f is evaluated from equation (4a) where $\nabla_s P$ is a linear combination of the pressures at the triangle vertices. Finally, in agreement with equation (4b), the exchange terms $q^{\pm}$ are modeled as

$$q^{\pm} = \sum_j \frac{2A_j}{\mu\omega_j}(P^{\pm} - P_f) \qquad (21c)$$

where the summation runs over the triangles T_j intercepting Ω_f; A_j is the area of $\Omega_f \cap T_j$. The balance equations (21a) and (21b) yield three linear equations with the same form as equation (20).

[52] More complex situations occur at the intersection of two or three fractures. Four or eight matrix control volumes are then in contact with Ω_f, each of them exchanging fluid with the fractures through two or three interfaces. On the other hand, on a fracture edge, a single matrix control volume surrounds Ω_f, with fluid exchange through two interfaces. Equations (21a)–(21c) can be straightforwardly extended to handle such situations.

[53] It should be mentioned here that for fractures with small cross resistance ($\omega' < 1$), the pressures $P_{\pm}$ on the faces are always very close to P_f, as can be expected. However, this means that fluid can be quasi-instantaneously transferred between the fracture and the matrix in the neighboring control volumes $\Omega^{\pm}$. Thus a storage volume per unit area of fracture of the order of $\delta_M \epsilon_m C_m$ is added to the theoretical value $b\epsilon_f C_f$. Although the flow rate along the fracture in a stationary situation is not modified, this results in a large decrease of pressure diffusivity, with an apparent diffusivity coefficient

$$\hat{D}_f \approx \frac{b\epsilon_f C_f}{\delta_M \epsilon_m C_m} D_f = \frac{\eta}{\delta'_M} D_f \qquad (22)$$

This effect will be illustrated on an example in section 5.

3.2.3. Intersection of the Well With Surface and Volume Elements

[54] The well is treated as a one-dimensional highly conductive system superimposed on the medium. Accordingly, it can be viewed as a line source or sink in the fractured porous medium, decomposed into elementary parts corresponding to its intersections with the grid surface and volume elements. Thus the approach which has recently been successfully implemented by *Sudicky et al.* [1995] is generalized here to unstructured meshes; moreover, the well does not necessarily follow edges of the mesh.

[55] If the well intercepts a control volume, the source terms involving J_w in equations (2) and (6) have to be added to the balance equations (19) and (21b). Recall that the pressure in the well is given at the midpoints of the segments contained in the tetrahedral volume elements and at the intersections of the well with the fractures (see Figure 2c). Therefore we need to model the exchanges between the well and the fractured medium, in order to relate J_w to the instantaneous pressures in the well and in the surrounding mesh points.

[56] Consider first the simple case of a well crossing at $\mathbf{w}$ a triangular element T on a fracture with vertices $\mathbf{w} + \mathbf{r}_i$, $i = 1, 2, 3$. Denote by P_w and P_i the pressures at $\mathbf{w}$ and $\mathbf{w} + \mathbf{r}_i$, respectively (Figure 2d). The well radius r_w is assumed to be negligible in comparison with the triangle size δ_M.

[57] It is natural to model the pressure field in T as the superposition of a global trend, induced for instance by a large-scale transverse flow and represented in T by a constant pressure gradient $\mathbf{G}$ and of a disturbance induced by the presence of the well, modeled according to analytical solutions. For a linear well in a closed reservoir with permeability K (in the pseudo steady regime), or in an unbounded homogeneous medium (for time t large in comparison with r^2/D), the pressure field at distance r from the well is given by (see section 4)

$$P(r,t) = P_w(t) + \frac{\mu J_w(t)}{2\pi K} \ln\left(\frac{r_w}{r}\right) \qquad (23)$$

Assuming that sufficient time has elapsed since the beginning of the well test, so that equation (23) is applicable, this superposition yields the pressure at the triangle vertices

$$P_i(t) = P_w(t) + \mathbf{G} \cdot \mathbf{r}_i + \frac{\mu b J_w(t)}{2\pi\sigma} \ln\left(\frac{r_w}{r_i}\right) \qquad (24)$$

[58] Equation (24) can be solved to obtain J_w as a linear combination of the differences $P_w - P_i$, which is the desired relationship. Furthermore, the flux J_w from the well to the surface element T can be distributed among the control surfaces containing the three triangle vertices in proportion to the corresponding differences $P_w - P_i$ (see Figure 2d)

$$J_{w,i} = \frac{P_w - P_i}{\langle P_w - P_j \rangle_a} J_w = a_i J_w \qquad (25)$$

where a_i is the areal coordinate of $\mathbf{w}$ in T [*Huyakorn and Pinder*, 1983] and $\langle \ \rangle_a$ denotes an average weighted by the a_i. The quantity $b J_{w,i}$ can be directly added to the right-hand side of the discretized equation (20).

[59] A similar approach can be applied to the interaction of a well segment with a matrix volume element (Figure 2e). Suppose a well segment of length l centered at $\mathbf{w}$ is contained in a tetrahedral volume element Θ. The model is still based on the theoretical result (23), and the pressures at the tetrahedron vertices are given by

$$P_i(t) = P_w(t) + \mathbf{G} \cdot \mathbf{r}_i + \frac{\mu J_w(t)}{2\pi K_m} \ln\left(\frac{r_w}{\beta r_i}\right) \qquad (26)$$

where β is a geometrical factor accounting for the difference between the distance r_i from the vertices to the midpoint $\boldsymbol{r_w}$ of the well segment and the projected distance from the vertices to the well. For unstructured meshes, β may be evaluated as an averaged cosine of the angle between $\boldsymbol{r_i}$ and well direction. As equation (24), (26) can be solved to obtain J_w as a linear combination of the differences $P_w - P_i$. Then the total flux J_w from the well segment to the matrix in the tetrahedron is distributed among the control volumes containing the four vertices of Θ in proportion to the corresponding differences $P_w - P_i$ (see Figure 2e)

$$J_{w,i} = \frac{P_w - P_i}{\langle P_w - P_j \rangle_v} J_w = v_i J_w \tag{27}$$

where v_i is the volume coordinate of $\boldsymbol{w}$ in the tetrahedron [*Huyakorn and Pinder*, 1983] and $\langle \ \rangle_v$ denotes an average weighted by the v_i. The quantity $l\,J_{w,i}$ can be directly added to equation (20).

[60] Note that when using equation (23), it was implicitly assumed that the porous matrix or the fracture is homogeneous or at least that their properties do not vary significantly in the neighborhood of the surface or volume element. Although the technique is formally applicable without modifications in heterogeneous media, since only local characteristics are used in equations (23)–(27), accurate results cannot be expected unless the characteristic length scale of inhomogeneities is large in comparison with the typical element size δ_M; however, this is a general requirement for a satisfactory description of any heterogeneous medium, even in the absence of a well.

[61] In case of large heterogeneities, a possible way to introduce a first order correction could be the technique used by *Durlofsky* [2000], in a similar context. The productivity index W, related to the coefficient of J_w in equations (23), (24), and (26), is evaluated for a model configuration made up of two concentric homogeneous regions. The outer one has the macroscopic effective properties of the heterogeneous medium; the inner one has a radius of the order of the heterogeneity length scale and properties obtained from a local average of the medium properties near the well. Thus the resulting well flux/well pressure relationship (i.e., the productivity index) is modified merely by the introduction of a skin coefficient, positive or negative. However, this first-order correction is not used here.

3.2.4. Flow in the Well

[62] The flow in the well is governed by equation (9), which provides an equation relating the pressures at the midpoints of the well segments and at its intersections with fractures. It is discretized in the usual way. Consider a point p on the well, and denote $d^{\pm}$ the distance to the neighboring points $p \pm 1$. Then

$$\frac{K_w}{\mu}\left(\frac{P_{p+1} - P_p}{d^+} - \frac{P_p - P_{p-1}}{d^-}\right) - h_p J_{w,p} = 0 \tag{28a}$$

where h_p is the length l of the well segment in the tetrahedron containing p, or b if p is at the intersection with a fracture. J_w is the linear combination of P_p and of

the pressures at the surrounding mesh points obtained by solving equations (24) or (26). At the well head $p = 1$, the equation is modified to incorporate the head flow rate Q_w

$$\frac{K_w}{\mu}\left(\frac{P_2 - P_1}{d^+}\right) - h_1 J_{w,1} + Q_w = 0 \tag{28b}$$

[63] In the following, pressure variations along the well are neglected. Hence a single well pressure P_w can be defined, and fluid conservation along the well can be written as

$$\sum_p h_p J_{w,p} = Q_w \tag{29}$$

3.3. Solution of the Discretized Equations

[64] Time derivatives are discretized to first order, in a fully implicit formulation. Since the matrix for the set of linear equations to be solved at each time step is not symmetric because of the exchange terms with the well (25) and (27), a biconjugate gradient algorithm is used.

[65] As is usual with diffusion equations, the time step δt has to satisfy the criterion

$$D\,\delta t \sim h^2 \tag{30}$$

where h is the typical space discretization scale and D is the diffusivity. In view of the contrast between the diffusivities of the fractures and matrix, this condition cannot be fulfilled everywhere. In practice, we used $\delta t \sim \delta_M^2/4D_f$ for the simulations of the early stages of the drawdown tests, in order to describe in detail the flow along the fractures. Later, when the pseudo steady regime is reached, larger time steps $\delta t \sim \delta_M^2/\eta D_f$ were used. The product ηD_f is a global diffusivity coefficient estimated by neglecting the matrix permeability and the fracture storage.

[66] Note that δt is always much larger than b^2/D_f. This is in agreement with equation (21c), which corresponds to a steady cross-fracture flow.

4. Comparison With Analytical Solutions

[67] A few simple cases have analytical solutions, which can be used as references to assess the performance of the numerical model.

[68] A first standard test case for any well model is the so-called drawdown test for a single vertical well in a uniform porous medium without any fracture, initially at rest, at a given constant pumping rate J_w per unit length of the well. In such a situation, the flow is two dimensional, and therefore it is not influenced by the periodicity condition along z.

[69] For a transversally unbounded medium, the transient solution for the pressure $P(r,t)$ at a distance r from the well is given by [see, e.g., *Streltsova*, 1988]

$$P(r,t) = -\frac{\mu J_w}{4\pi K_m}\text{Ei}\left(-\frac{r^2}{4D_m t}\right) \tag{31}$$

where the exponential integral function Ei(x) is defined as [see *Gradshteyn and Ryshik*, 1965]

$$Ei(x) = \int_{-\infty}^{x} \frac{e^t}{t} \, dt \qquad (32)$$

After a short initial period, equation (31) reduces to the well-known approximate logarithm form

$$P(r,t) = \frac{\mu J_w}{4\pi K_m}\left(\ln\frac{4D_m t}{r^2} + 0.81\right), \qquad \left(\pm 1\% \text{ for } t > \frac{100 r^2}{4D_m}\right) \qquad (33)$$

P represents the well pressure if r is equal to r_w in equations (31) or (33).

[70] Another basic solution is the pseudosteady long-time solution for a finite region with drainage area A [*Bourdarot*, 1996; *Earlougher*, 1977]

$$P(r,t) = \frac{J_w t}{\epsilon_m C_m A} + \frac{\mu J_w}{4\pi K_m}\left(\ln\frac{A}{r^2} + \ln\frac{2.2458}{C_A}\right), \qquad (34)$$

where C_A is a shape factor which depends on the reservoir geometry and on the location of the well. It is provided by *Bourdarot* [1996] and *Earlougher* [1977] for a variety of situations, together with the minimum time when it becomes applicable. The term independent of time in equation (34) allows one to evaluate the medium properties in the finite flow region.

[71] Finally, *Carslaw and Jaeger* [1959] provide a general solution for the 2-D axisymmetric well problem, with flow or pressure conditions at the well surface and at any cylindrical outer boundary. For instance, for a well with constant pressure P_w in an unbounded medium,

$$P(r,t) = P_w + \frac{2P_w}{\pi}\int_0^{\infty} \frac{J_0(xr)Y_0(xr_w) - Y_0(xr)J_0(xr_w)}{J_0^2(xr_w) + Y_0^2(xr_w)} e^{-D_m tx^2}\frac{dx}{x}, \qquad (35)$$

where J_0, Y_0 denote the conventional Bessel functions of zero order. The corresponding total instantaneous well flux may be approximated by

$$J_w(t) = 4\pi K_m\left(\vartheta - \gamma\vartheta^2\right) \qquad (36)$$

for $\theta_D = 4 D_m t/r_w^2 \gg 1$, where $\vartheta = (\ln \theta_D - 2\gamma)^{-1}$ and $\gamma = 0.57722\ldots$ is Euler's constant.

[72] The results of test runs are compared in Figures 3 and 4 with these analytical solutions. The domain was a cubic region of size L, containing a uniform medium and crossed by a straight well of length L. The data are presented in terms of the dimensionless time t_{DA} based on the drainage area $A = L^2$

$$t_{DA} = 4D_m t/L^2 \qquad (37a)$$

When the flux J_w is imposed, the dimensionless pressure $P_{w,DA}$ is defined as

$$P_{w,DA} = \frac{4\pi K_m}{\mu J_w} P_w \qquad (37b)$$

When the well pressure is imposed, the dimensionless flow rate $J_{w,DA}$ is defined as

$$J_{w,DA} = \frac{\mu}{4\pi K_m P_w} J_w \qquad (37c)$$

[73] The calculations in Figure 3 have been carried out with periodicity conditions. The discretization size δ_M, the time step δt and the horizontal location x_w of the well have been varied. The well radius is $r_w = L/300$. The analytical result (33) applies for early times, i.e., before the pressure fields of the periodic replicas of the well overlap.

[74] The data in Figure 3a correspond to $\delta t_{DA} = 4/900$, with $\delta_M/L = 1/9$, $1/12$ and $1/18$, and a constant flow rate J_w. The well pressure is plotted as a function of the dimensionless time t_{DA}. The agreement with the analytical result (33) improves when the discretization is refined from $\delta_M = L/9$ to $\delta_M = L/12$, and then slightly deteriorates when δ_M is further decreased to $1/18$. However, the deviations from equation (33) never exceed 4% in the range $0.01 \le t_{DA} \le 0.2$ even for $\delta_M = L/9$.

[75] In Figure 3b, the flow rate J_w is kept constant, $\delta_M = L/12$, and the time step is varied, with $\delta t_{DA} = 16/900$, $8/900$, and $4/900$, i.e., $D_m\delta t/\delta_M^2 = 0.64$, 0.32, and 0.16, respectively. The influence of this variation on the calculated well pressure is very small, with less than 3% difference between $\delta t_{DA} = 16/900$ and $4/900$ when $t_{DA} \le 0.1$, and almost vanishes when $t_{DA} \ge 0.1$.

[76] In Figure 3c, $\delta_M = L/12$, and $\delta t_{DA} = 0.009$ ($D_m \delta t/\delta_M^2 = 0.32$), with a constant flow rate J_w, but three different well locations x_w are considered. Because of the periodic boundary conditions, the three calculations are in principle equivalent. However, the well crosses the elements of the unstructured mesh at different locations, which results in different discretizations of the well, with different sets of well segments. The comparison of the three curves shows that the resulting well pressure may vary by about ±1%, which is of the order of the influence of the changes of δ_M in Figure 3a. The same comments apply to Figure 3d, where the same parameters were used to compute $J_{w,DA}$ as a function of t_{DA} for a constant well pressure P_w.

[77] The small deviation of the numerical data in Figure 3 from the analytical solution (33) may result from at least three reasons. Two of them are related to the description of the fluid exchanges between the well and the surrounding medium. First, the rule applied in equations (25) and (27) to distribute the flux J_w among the neighboring control volumes is partly arbitrary. Second, the use of a single average coefficient β in equation (26) is also an approximation. However, the main reason is probably the first-order discretization of equation (19), which assumes piecewise constant pressure gradient and velocity over the mesh elements (except in the elements that intercept the well, where this linear approximation is replaced by the analytical development (24)). The influence of the first and last approximations should decrease as the discretization is refined; however, the convergence toward the exact solution is not monotonous (see Figure 3a), because some randomness is introduced by the location of the well intersection with the mesh elements. The influence of using an average β is not directly related to δ_M, but the present data show that it is negligible. Recall, in addition, that this approximation is
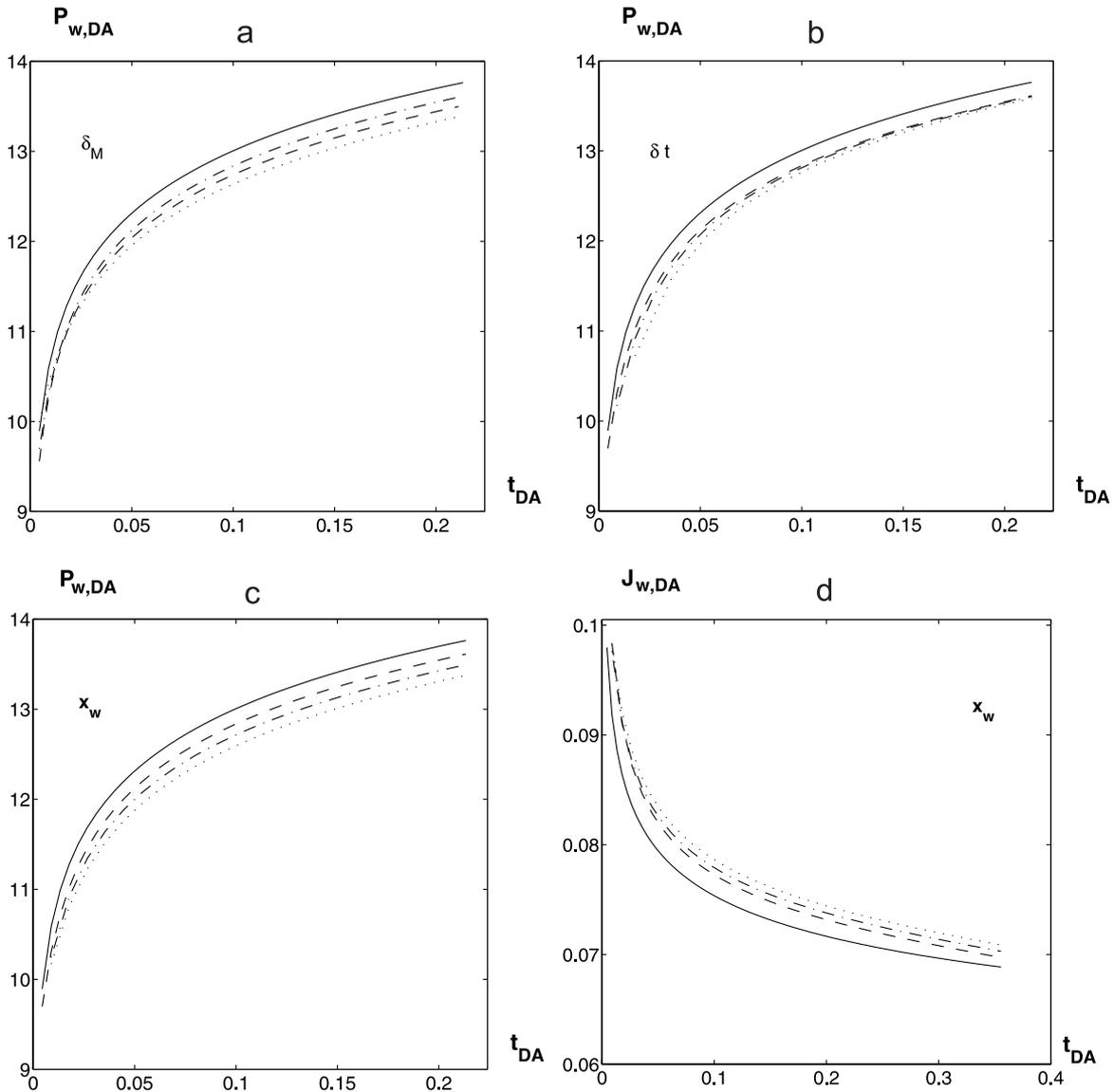
Figure 3. Comparison of numerical simulations for a straight well in a cubic domain with size L and periodicity conditions, with the analytical result (33) (solid curves). The well pressure $P_{w,DA}$ for a constant flow rate J_w (a,b,c) and the flow rate $J_{w, DA}$ for a constant well pressure P_w (d) are plotted versus time t_{DA}. In Figure 3a, $\delta t_{DA} = 4/900$, and $\delta_M/L = 1/9$ (dotted curves), 1/12 (dash-dotted curves), and 1/18 (dashed curves). In Figure 3b, $\delta_M = L/12$ and $\delta t_{DA} = 16/900$ (dotted curves), 8/900 (dash-dotted curves), and 4/900 (dashed curves). In Figures 3c and 3d, $\delta_M = L/12$, and $\delta t_{DA} = 0.009$, and the three discontinuous curves correspond to different locations of the well in the unit cell.

not used to describe the intersection of fracture surface element with the well (compare equations (24) and (26)).

[78] The calculations in Figure 4 correspond to a uniform medium in a closed domain of size L, with $r_w = L/400$, $\delta_M = L/16$, and $\delta t_{DA} = 0.04$. In case 1, the vertical well is located on the axis of the cell, i.e., at distance $L/2 = 8\delta_M$ from the four lateral boundaries. In case 2, it is midway between the axis and one of the walls (at a distance $L/4 = 4\delta_M$ from a wall), and in case 3, it is midway between the axis and one of the angles, i.e., at a distance $L/4 = 4\delta_M$ from two walls.

[79] For early times, the results can be successfully compared with the analytical solution (33) in an unbounded medium. The location of the well does not matter, since the influence of the impervious boundaries is not felt by the flow. However, the curve for case 3 deviates from equation (33) sooner than cases 1 and 2, because the well is closer to a corner of the closed reservoir. For longer times, all the curves converge towards the corresponding pseudo steady solutions (34), with the shape factors C_A given by *Earlougher* [1977].

5. Straight Well Intersecting a Single Fracture

[80] A well intersecting a single fracture is a basic case which has also given rise to analytical results and which can constitute the basis for modeling more complex situations.

[81] Let us first mention the case of a single fracture, bounded or unbounded, in an impervious medium. Flow is
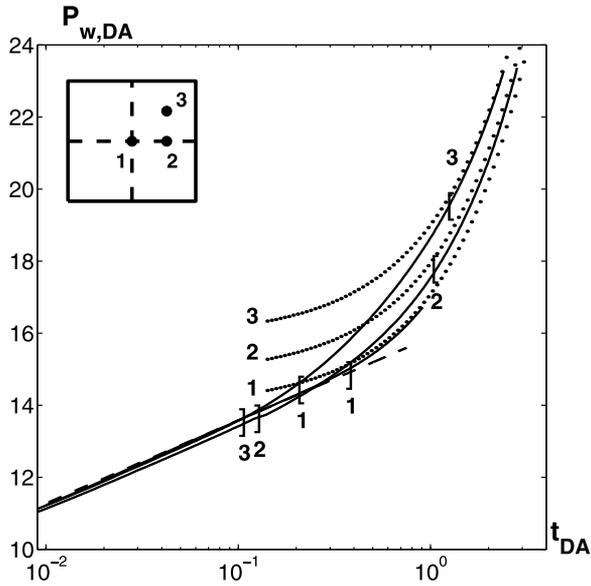
Figure 4. The well pressure $P_{w,DA}$ for a constant flow rate J_w versus time t_{DA}. Numerical results computed in a closed cubic domain of size L, with $\delta_M = L/16$ and $\delta t_{DA} = 0.04$ (solid curves); analytical results (33) (dashed curves) and (34) (dotted curves). Curves labeled $(1-3)$ correspond to different positions of the well in the drainage region, as depicted in the insert. Brackets indicate the ranges of validity within $\pm 1\%$ of the infinite medium (33) and pseudo steady (34) solutions, as given by *Earlougher* [1977].

restricted to the fracture volume. The problem is formally equivalent to the 2-D situations addressed in section 4; equations $(31)-(35)$ apply with the matrix properties K_m, D_m, ϵ_m, and C_m replaced by the corresponding quantities for the fracture.

[82] To our knowledge, no general transient solution was provided yet for the general case of a well intercepting a finite single fracture in a permeable porous medium, with well/matrix, well/fracture, and fracture/matrix exchanges.

[83] Hydraulically generated fractures, highly conductive and generally parallel to the well have received considerable attention [see, e.g., *Gringarten and Ramey*, 1974; *Gringarten et al.*, 1974; *Streltsova*, 1988, and references therein]. Analytical solutions generally assume either a uniform pressure or a uniform surface exchange rate with the matrix in the fracture. A transient regime takes place generally, with fracture pressure variations proportional to time at power t^n, with $0.25 \leq n \leq 0.5$. Later on, the well/ fracture system behaves like a well with a larger effective radius.

[84] *Boulton and Streltsova* [1977b] considered periodic parallel infinite fractures with spacing H, intercepting a well at right angle. Fluid is drained from the matrix material through the fractures; direct well/matrix exchanges and radial flow in the matrix are ignored. For very conducting fractures, three regimes can be distinguished. At early times, flow is mainly due to fracture compressibility; as mentioned above, it is governed by an equation of the form (31), based on the fracture properties. For intermediate times, matrix provides fluid to the fracture, where the pressure varies at a slower rate, with the prefactor in equation (33) divided by

about 2. Such a behavior is also observed in other transient situations, for instance, with a well crossing a single fracture [see *Weir*, 1999]. The factor 1/2 is related to the hypothesis of no radial flow in the matrix, and other models would yield slightly larger coefficients [*Young*, 1992]. Finally, at late times, matrix and fracture pressures at a given radial distance equilibrate, and equation (31) applies again, with a modified diffusivity D_s which accounts for the fracture permeability and for the composite storage in the fracture and in the matrix

$$D_s = \frac{D_f}{1 + \frac{H\epsilon_m C_m}{b\epsilon_f C_f}} \qquad (38)$$

[85] Simulations have been run in such a geometry, with a fracture normal to the well which crosses the whole unit cell. Periodicity is applied in the direction of the well, and the spacing H is equal to the cell size L. However, periodicity is also applied in the transverse directions. Therefore the simulations correspond to a closed reservoir, with $L \times L$ drainage area, instead of the unbounded domain in the derivation of *Boulton and Streltsova* [1977b]. The fracture size R is defined as $R = L/2$, and therefore $L' = L/R = 2$ and the dimensionless times t' in equation (15a) and t_{DA} in equation (37a) are equal.

[86] Two simulations were conducted, with or without taking into account the well/matrix exchanges. A constant flow rate Q_w is applied, and the numerical results are presented in terms of the dimensionless pressure $P_{w,DA} = 4\pi K_m L P_w/\mu Q_w$ and of its derivative with respect to the logarithm of time, $\Pi_{w,DA} = dP_{w,DA}/d \ln t'$ (see equation (37)). The results for $\delta_M' = 1/8$, $b' = \eta = 5 \times 10^{-4}$, $r_w' = 5 \times 10^{-3}$, and $\sigma' = 50$ are plotted against t' in Figure 5.

[87] The first observation is that the curves with or without well/matrix exchanges do not differ much. With the parameters used here, they are widely dominated by the flow through the fracture.

[88] Owing to the lateral no-flux boundaries, P_w is not expected to exactly obey the same three regimes as in the *Boulton and Streltsova* [1977b] solution. At early times, when flow is confined in the fracture, an additional transition should take place at $t \sim L^2/4 D_f$ ($t' \sim D_m/D_f = \eta/\sigma' = 10^{-5}$) between the logarithmic and linear behaviors, (33) and (34), when the pressure wave reaches the cell boundaries. This is indeed observed in Figure 5.

[89] After a very brief transient (region A in Figure 5), there is a plateau in the curves for $\Pi_{w,DA}$ (region B), which corresponds to the values predicted by equation (33), namely, $L'/\sigma' = 1/25$ $((\mu Q_w/b)/(4\pi K_f) = \mu Q_w/4\pi R K_m \sigma' = (\mu Q_w)/(4\pi L K_m)$ $(L'/\sigma'))$ without well/matrix exchanges or about $L'/(L' + \sigma') = 1/26$ with well/matrix exchanges, respectively. This plateau is followed by a steeper increase (region C), where the slope of $\Pi_{w,DA}$ versus t' is about 0.78, in a logarithmic plot, which means that $P_{w,DA}$ grows as $t'^{0.78}$. If the porous matrix were impervious, the pressure would increase linearly with time at this stage, according to equation (34).

[90] However, owing to the excessive storage in the fracture which results from the discretization (see section 3.2.2), these two events last for too long a time. Based on D_f, the pressure wave should reach the cell boundary at $t' \sim 10^{-5}$, whereas the plateau of $\Pi_{w,DA}$ lasts until $t' \sim 10^{-3}$. The
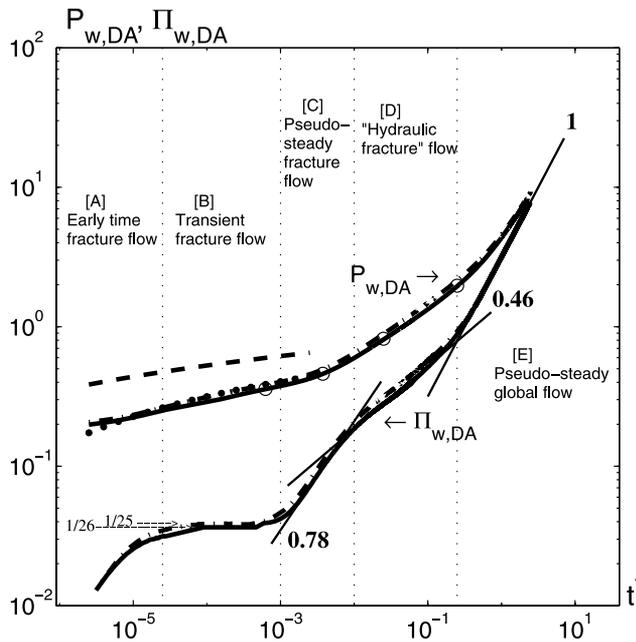
Figure 5. The well pressure $P_{w,DA}$ and its logarithmic time derivative $\Pi_{w,DA}$ versus the dimensionless time t', for a straight well intersecting a series of parallel plane fractures, with spacing $H = L$, in a closed reservoir with a square drainage area $L \times L$. Data are for $r'_w = 5 \times 10^{-3}$, $\sigma' = 50$, $b' = \eta = 5 \times 10^{-4}$, and $\delta'_M = 1/8$. Curves correspond to $P_{w,DA}$ and $\Pi_{w,DA}$ with (solid curves) or without (dash-dotted curves) well/matrix exchanges, and to the analytical prediction (32) for $P_{w,DA}$ based on D_f (dashed curves) or on $\hat{D}_f$ in equation (22) (dotted curves). Straight lines indicate fitted slopes 0.78, 0.46 and 1. Horizontal arrows correspond to the values of the plateau of $\Pi_{w,DA}$ predicted by equation (33), with or without well/matrix exchanges. Open circles show the times corresponding to the four stages in Figure 6.

analytical solutions from equation (32) based on the theoretical diffusivity D_f or on the modified diffusivity $\hat{D}_f$ in equation (22) are plotted in Figure 5. The latter curve is in very good agreement with the numerical results in the transient fracture flow period.

[91] Later on, flow in the matrix becomes significant, and another regime is reached (region D). The slope of the curve of $\Pi_{w,DA}$ is about 0.46, up to $t' = 1/4$, which is of the order of the typical time $t' \sim 1$ ($t \sim H^2/4D_m$) for the pressure wave to travel from the fracture to the middle of the matrix layer. This regime corresponds to a power dependence of P_w on time as $t^{0.46}$, as observed with hydraulic fractures, rather than to the halved logarithmic law of *Boulton and Streltsova* [1977b], again because of the domain impervious boundaries. Finally, another pseudo steady regime is reached for $t' > 1/4$, with a law of the form of equation (34) (region E).

[92] Two hydraulic conductivities can be measured from the well pressure curve, in the first and last regimes described above. First, the plateau B of $\Pi_{w,DA}$ provides the fracture conductivity, as already mentioned. Note that its value is not influenced by the exaggerated fracture storage. Second, in the final pseudo steady regime E, P_w increases linearly with time (see equation (34)). An extrapolation at

zero time of this linear law provides an estimate of a global effective permeability K_{eff} for the fractured medium.

[93] In situations where the reservoir size L is large in comparison with the scale R of the fractures (which is not satisfied here), the fractured medium at sufficient distance from the well can be viewed as an equivalent homogeneous medium. K_{eff} is then an estimate of its permeability. It is shown in section 6 that it is directly related to the effective permeability of the fractured porous medium determined by *Koudina et al.* [1998] for steady state flow.

[94] For illustration, the pressure at the mesh points is plotted as a function of the distance $r' = r/R$ from the well in Figure 6 at various times in the four successive regimes, when exchanges are allowed between well and matrix. At the end of the initial transient flow in the fracture (Figure 6a), and even in the subsequent pseudo steady period (Figure 6b), pressure in the matrix remains at its initial value, except in the close vicinity of the well. The analytical prediction of *Boulton and Streltsova* [1977a] at early time for the pressure in the fracture based on $\hat{D}_f$ in equation (22) is also plotted in Figure 6a. It is in excellent agreement with the numerical results.

[95] Later, during the third period, pressure in the fracture is much more uniform (Figure 6c). Pressure in the matrix increases, according to the distance from the fracture. Owing to the advancing front technique used for the mesh generation, the mesh points tend to arrange in a series of layers parallel to the fracture plane, and the corresponding pressures form a family of curves. Pressure at the point closest to the fracture has already started to increase, while the part of the matrix most remote from the fracture is still unaffected. Finally, in the global pseudo steady regime, pressure increases linearly with time throughout the medium. Its variations with the radial distance r from the well and with the vertical distance from the fracture are of similar orders of magnitude.

6. Well Through a Fractured Porous Medium

6.1. Fracture Network Model

[96] We consider here randomly fractured media, as modeled by *Huseby et al.* [1997]. The fractures are plane polygonal objects, randomly located and oriented in space. In the present case, they are regular hexagons, inscribed in disks of radius R. An infinite network is obtained by a periodic reproduction of a cubic unit cell of size L^3 in the x-, y- and z-directions. An example is displayed in Figure 1b, which contains 17,643 nodes, 222,820 triangles, and 111,410 tetrahedra.

[97] The density of fractures is quantified by the dimensionless parameter ρ', which is the number of fractures per excluded volume V_{ex}, equal to $9\sqrt{3}R^3/2$ for hexagons [see *Huseby et al.*, 1997; *Adler and Thovert*, 1999]. ρ' is also a measure of the connectivity of the fracture network, since it is the mean number of fractures intersecting a given fracture. In particular, ρ' determines the percolation of the fracture network, with a percolation threshold $\rho'_c \approx 2.3$. For $\rho' > \rho'_c$, a connected set of fractures exists which spans the whole medium. For $\rho' < \rho'_c$, the fractures are isolated or in small disconnected clusters. *Bogdanov et al.* [2002] have shown that this has a dramatic influence on the macroscopic permeability of the fractured medium. Percolating clusters are preferential flow paths throughout the medium, whereas
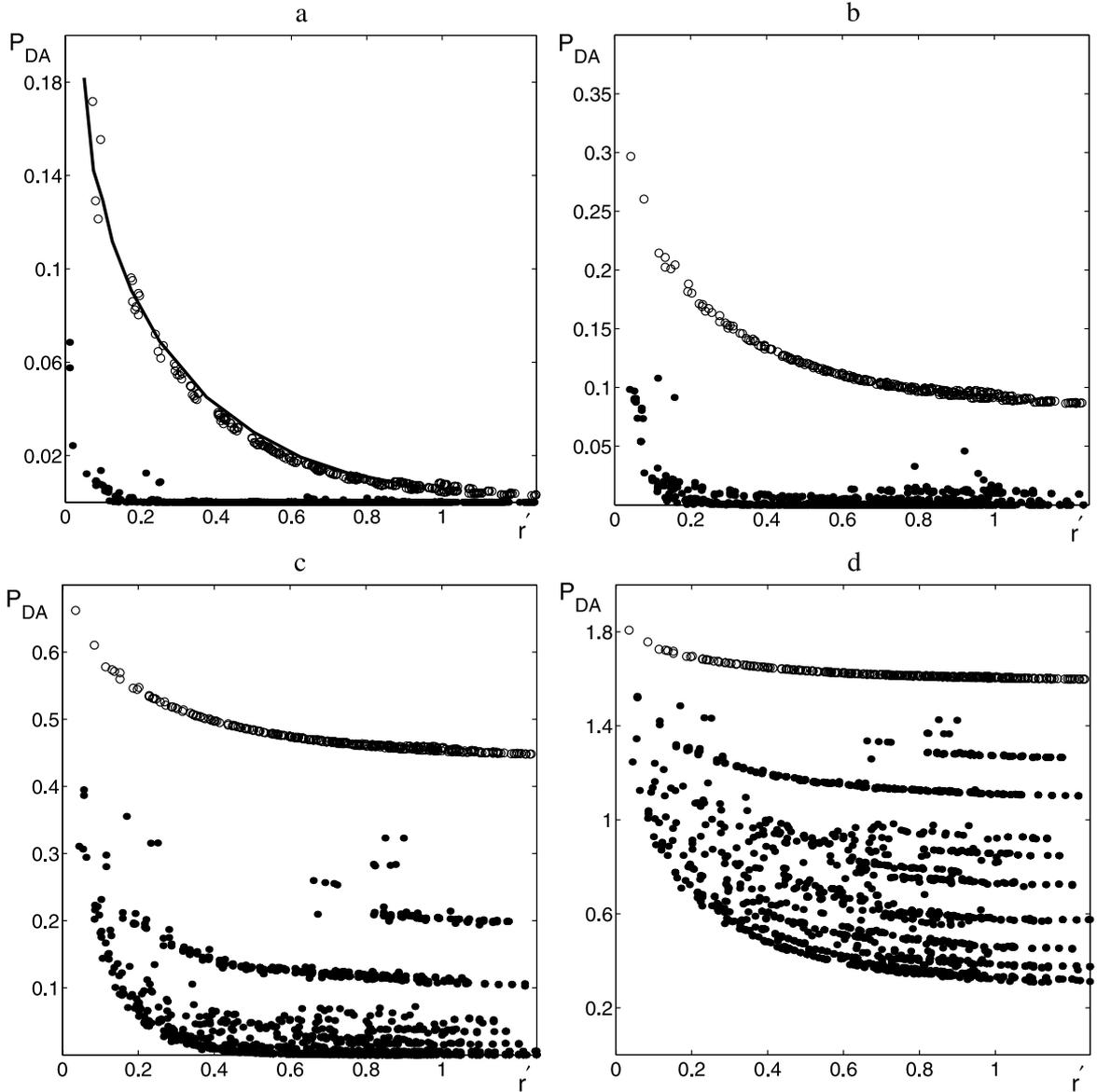
Figure 6. The pressure P_{DA} at the mesh points on the fracture (open circles) and in the matrix (solid circles) as a function of the radial distance r' to the well. The data correspond to the simulations in Figure 5, including direct well/matrix exchanges, at the times marked on the curve for $P_{w,DA}$, $t' = 6.25 \times 10^{-4}$ (a), 3.75×10^{-3} (b), 0.025 (c) and 0.25 (d). The solid curve in Figure 6a is the complete series solution for the pressure in the fracture from *Boulton and Streltsova* [1977a], based on $\hat{D}_f$.

isolated fractures merely facilitate fluid flow over short distances.

[98] For very conducting fractures, it is expected that the number n_I of intersections of the well with the network is a key parameter for the flow, since it conditions the fluid exchanges. Its statistical properties can be derived as follows. The mean number N_I of well intersections with fractures in the unit cell can be evaluated from the volumetric surface area $\mathcal{S}$ of the fracture network, which is given for hexagons by [*Adler and Thovert*, 1999]

$$\mathcal{S} = \frac{\rho'}{3R} \qquad (39)$$

After averaging over the fracture orientations relative to the well direction, one obtains

$$N_I = \frac{\rho' L}{6R} \qquad (40)$$

Conversely, the mean spacing between the intersections is

$$S_I = \frac{6R}{\rho'} \qquad (41)$$

Since the fractures are located according to a Poisson process, their intersections with the well are also Poissonian. Thus n_I obeys a Poisson law with parameter N_I, and the spacings s_I obey a negative exponential law with parameter $1/S_I$

$$\mathcal{P}(n_I = n) = \frac{N_I^n}{n!} e^{-N_I}, \qquad f(s_I) = \frac{1}{S_I} e^{-s_I/S_I} \qquad (42)$$
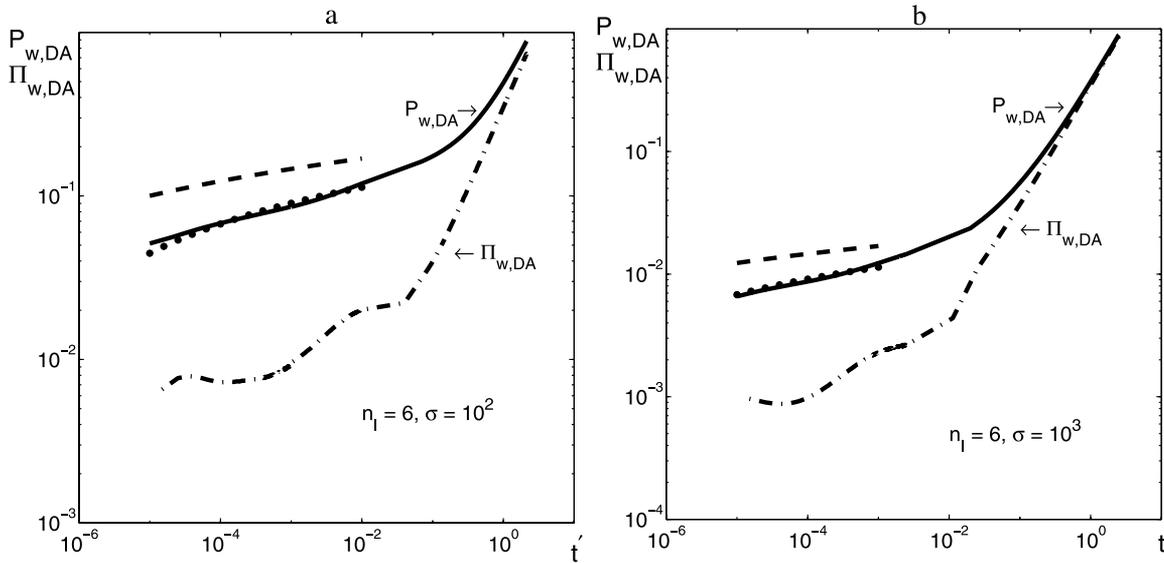
Figure 7. Pressure $P_{w,DA}$ (solid curves) and its derivative $\Pi_{w,DA} = \mathrm{d}P_{w,DA}/\mathrm{d}\ln t'$ (dash-dotted curves) for a pressure drawdown test, for a fracture network with $\rho' = 6$ in a unit cell with size $L = 6$. The well intersects $n_I = 6$ fractures. Data are for $r'_w = 0.01$, $b' = 10^{-3}$; $\sigma' = 10^2$ (a) and $\sigma' = 10^3$ (b). The analytical solution by *Boulton and Streltsova* [1977b] for a spacing equal to the mean value $S_I = R$ is given for the theoretical D_f (dashed curves) and for $\hat{D}_f$ (dotted curves).

These probability laws show that very small or very large numbers of intersections, compared with N_I, have small probabilities. For instance, the probability for $3 \leq n_I \leq 10$ ($7 \leq n_I \leq 17$) is about 0.9 for $N_I = 6$ ($N_I = 12$). However, the spacing distribution is very broad, with a large probability of small values.

6.2.   Examples of Pressure Drawdown Curves

[99] As a rule, all the typical flow regimes present in Figure 5 can be observed in the drawdown curves for wells in randomly fractured media. In particular, the two latest regimes, namely, the "hydraulic fracture" and the pseudo-steady flow, can always be clearly identified. However, the early and intermediate regimes are often blurred or do not show up at all, and additional features can appear in the curves.

[100] First, during the period when flow takes place mainly in the fractures, the pressure wave starts propagating in the fractures which cross the well and then spreads out in all the fractures connected to them. Of course, different curves are obtained according to whether the number n_I of intersections is smaller or larger than the expected value N_I. Also, fluid exchanges between the well and different parts of the fracture network may take place in parallel, but over different timescales. Recall that the number of fractures intersecting a given fracture is also a Poisson variable. Thus with, for instance, $\rho' = 4$, there is a probability about 0.09 that a fracture is connected to one or zero fractures and about 0.11 that it is connected to 7 or more fractures. Hence the drainage areas corresponding to the various parts of the network connected with the well can be quite different, which yields different onset times and durations for the pseudo steady fracture flow.

[101] As a whole, though, the influence of all these statistical fluctuations decreases with the network density ρ'. For $\rho' = 6$, the fractures are very interconnected; the

multiple paths from any point on the network to any other point allow fast communication and prevent the pressure to evolve in very different ways in different areas. For $\rho' = 4$, a small fraction of the fractures are not connected to any others. Finally, for $\rho' = 1.5$, most of the fractures are single or in pairs and behave independently.

[102] Typical results for a network with density $\rho' = 6$ are given in Figure 7 for $r'_w = 0.01$ and two values of the conductivity $\sigma' = 10^2$ and 10^3. In this case, the actual number n_I of intersections is equal to the expected value $N_I = 6$.

[103] The four flow regimes identified in Figure 5 can be observed here, i.e., transient and pseudo steady fracture flows, followed by transient and pseudo steady global flows. The decrease in the logarithmic time derivative $\Pi_{w,DA}$ at $t' \sim 10^{-4}$ is commonly observed and corresponds to the spread of the pressure wave in the ramified network, with decreasing hydraulic resistance.

[104] For illustration, the analytical solution by *Boulton and Streltsova* [1977b] for a spacing equal to the mean value S_I is also shown in Figure 7, for the theoretical D_f and for $\hat{D}_f$. With the correction for the fracture storage, the analytical solution for the case of parallel fractures yields a very good estimate of the well pressure during the transient fracture flow in this randomly fractured medium, for both values of σ.

6.3.   Effective Properties of the Fractured Porous Medium

[105] Simulations were run for fractured porous media in cells with size $L = 6\,R$, containing 41, 110, or 161 fractures. These values correspond to densities $\rho' = 1.48$, 3.97, and 5.81, respectively, and $N_I = \rho'$. A set of measurements for 100 different horizontal positions of the well head showed that the statistical properties (40)–(42) are satisfied.

[106] Pressure drawdown was simulated in each case with $r'_w = 0.01$, various fracture conductivities $\sigma' = 10$ to 1000,

and for various locations of the well head, which yield different numbers n_I of fractures intersected by the well. In the late pseudo steady stage, the well pressure always increases linearly with time. The results can be analyzed by comparison with the pressure response of a well in a homogeneous medium with permeability K_r and storage coefficient $\epsilon_g C_g$ (see equation (34))

$$P_w(t) = \frac{J_w}{\epsilon_g C_g A} t + \frac{\mu J_w}{4\pi K_r}\left(\ln\frac{A}{r_w^2} + \ln\frac{2.2458}{C_A}\right) \qquad (43a)$$

or in dimensionless form

$$P_{w,DA}(t) = \frac{4\pi R^2 \epsilon_m C_m}{A \epsilon_g C_g} t + \frac{1}{K_r'}\left(\ln\frac{A}{r_w^2} + \ln\frac{2.2458}{C_A}\right), \qquad (43b)$$

where $A = L^2$ and $C_A = 30.8828$ for a square drainage area [*Earlougher*, 1977].

[107] Least squares linear fits of the numerical data always yield a value of the slope in agreement with the expected value, with a relative error less than 10^{-3}. Thus the relative uncertainty on the intercept $P_{0,DA}$ with the ordinate axis is of the same order of magnitude, and K_r' can be deduced from $P_{0,DA}$ with the same accuracy

$$K_r' = \frac{\ln\left(A/r_w^2\right) + \ln(2.2458/C_A)}{P_{0,DA}} \qquad (44)$$

[108] This apparent global permeability relative to radial flow from the well is plotted in Figure 8, as a function of σ', for the three network densities ρ' and the various numbers n_I of well/fracture intersections. The figure also shows the macroscopic effective permeability K_{eff}' of the fractured media, relative to steady linear flow, as determined by *Bogdanov et al.* [2002] (see section 1).

[109] Clearly, for a given medium and a given conductivity, K_r strongly depends on n_I. As a rule, K_r is significantly larger than K_{eff}, except for small values of n_I, compared with the expected N_I, which are statistically unlikely (see section 6.1 and equation (42)). Hence K_r cannot be regarded as an intrinsic property of the fractured medium, since it depends on boundary conditions.

[110] On physical grounds, it can be expected that the well pressure response should depend on the far-field effective permeability of the medium, which can be identified as K_{eff}, and on the particular interactions of the well with the fracture network in a given situation. This can be modeled in a first approximation by introducing a skin factor S in equation (43)

$$P_{w,DA}(t) = \frac{4\pi R^2 \epsilon_m C_m}{A \epsilon_g C_g} t + \frac{1}{K_{eff}'}\left(\ln\frac{A}{r_w^2} + \ln\frac{2.2458}{C_A} + 2S\right) \qquad (45)$$

[111] Such a parameter appears in various situations [*Earlougher*, 1977]. Heterogeneities near the well, such as the ones caused by formation damage, can be described in this way. The skin factor S is positive (negative) if permeability around the well is smaller (larger) than in the surrounding medium. For instance, if permeability is K_a in a cylindrical
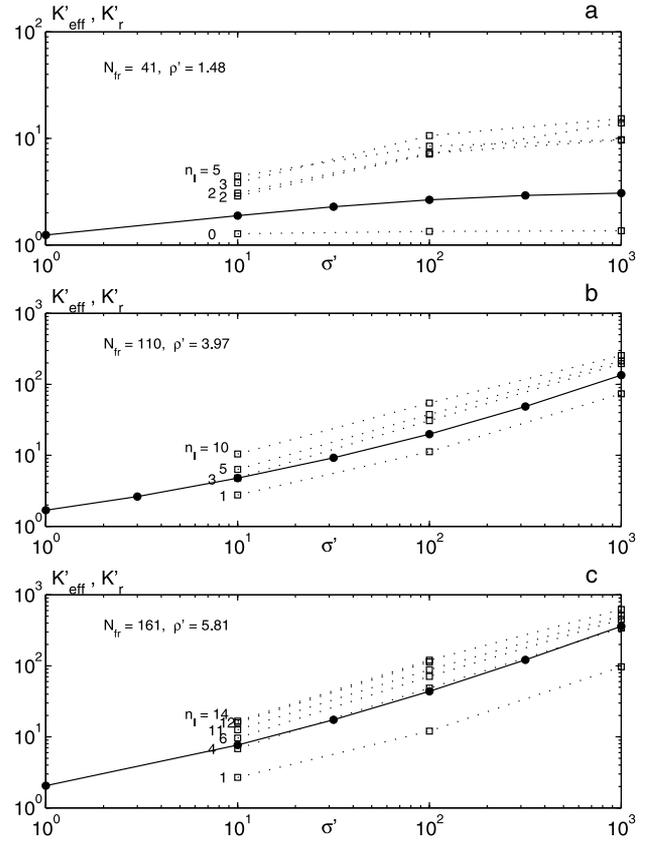
Figure 8. Effective permeability K_{eff}' (solid circles) and apparent permeability K_r' (open squares) for fractured media with $\rho' = 1.48$ (a), 3.97 (b) and 5.81 (c), as functions of the fracture conductivity σ'. Data are for a unit cell size $L = 6R$ and various numbers n_I of intersections of the well with the fracture network.

region with radius r_a around the well and K beyond this radius, S is given by

$$S = \left(\frac{K}{K_a} - 1\right)\ln\frac{r_a}{r_w} \qquad (46)$$

For late times and on a large scale, hydraulic fractures along the well also require such a correction.

[112] The value of S which results via equation (45) from the numerical value of P_0 was evaluated. It is plotted in Figure 9a as a function of the spacing between the well/fracture intersections normalized by its expected value, s_I/S_I. The spacing is a more intrinsic characterization of the well and fracture interconnections than the number n_I of intersections, because its statistical expectation and its standard deviation do not depend on the sample size. S increases with the spacing. A least square linear fit yields

$$S = 2.5\left(\frac{s_I}{S_I} - 1\right) - 1.6 \qquad (r = 0.963) \qquad (47)$$

[113] Of course, the data are somewhat scattered around the mean linear law (47), for several reasons. First, statistical fluctuations can be very important, especially for
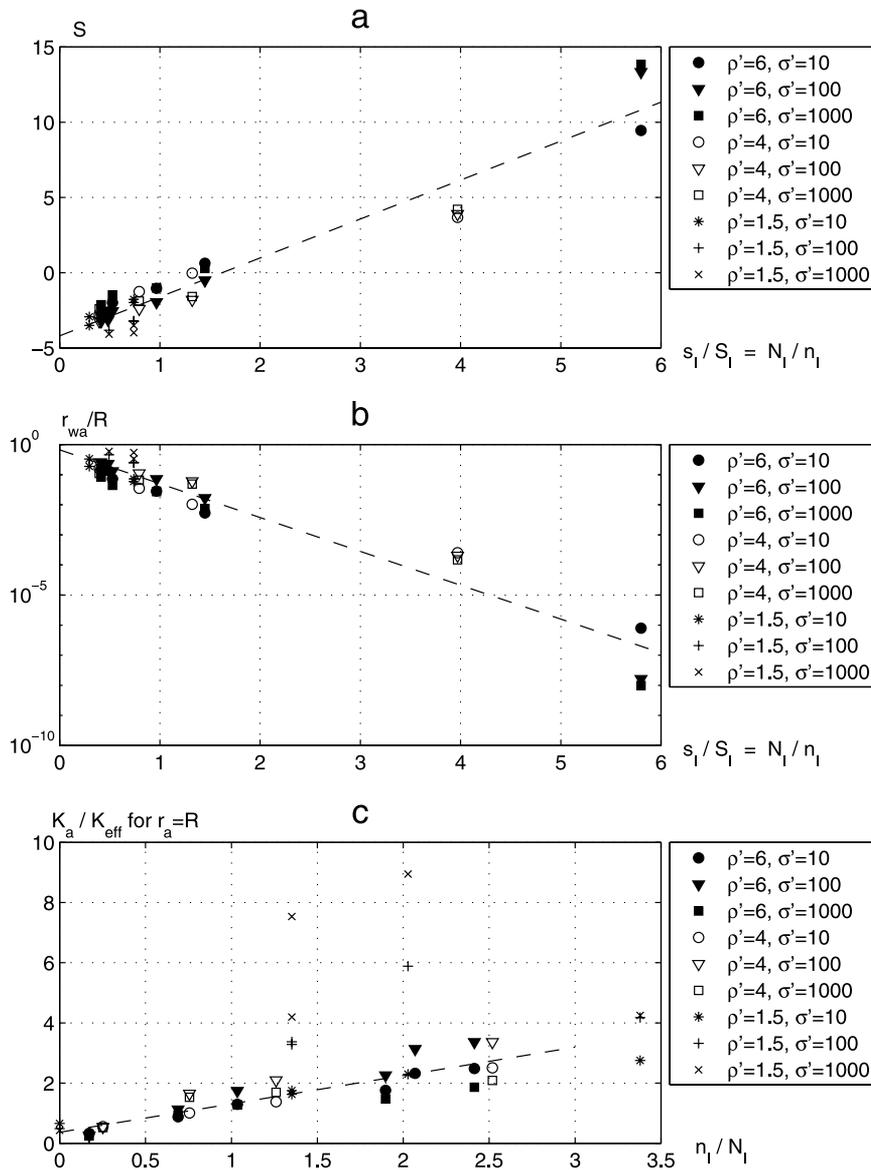
Figure 9. Coefficient S (a) and apparent well radius $r'_{w,a}$ (b) as functions of the spacing s_I/S_I; permeability ratio K_a/K_{eff} for $r_a = R$ as a function of the number of intersections n_I/N_i (c). Data are for a well with a radius $r_w = R/100$ in a randomly fractured medium, with various densities ρ' and fracture conductivities σ'. The broken lines correspond to the fit (47) in Figures 9a and 9b and to the fit (50) in Figure 9c.

small n_I (i.e., large spacings); for instance, if the well crosses a single fracture, the well pressure response is very sensitive to the connectivity of this fracture with the rest of the network. Second, S depends a priori on the fracture conductivity. For example, it should vanish for poorly conducting fractures. Only large conductivities σ' are considered here, but the value of S for $\sigma' = 10$ are generally smaller (in absolute value) than the values for $\sigma' = 10^2$ and 10^3, which are very similar. Finally, S can also depend on the network density ρ', in particular because of size effects when ρ' is not much larger than ρ'_c. In this case, the well intersects finite clusters of connected fractures, and S is expected to depend on the ratio of their typical size to the reservoir size L.

[114] Nevertheless, equations (45) and (47) provide a guideline for the prediction of the performances of a well,

given the effective properties $\epsilon_g C_g$ and K_{eff} of the fractured medium and the connectivity of the well with the fracture network, for highly conducting and well-connected fractures. The density of well-fracture intersections is generally readily available from well log data, whereas K_{eff} can be determined from the fracture network and matrix properties [*Bogdanov et al.*, 2002].

[115] Other representations of the same data are possible. They are based on a priori models for the interactions of the well with the fracture network, and do not bring any additional information with respect to equations (45), which is the raw result of the numerical simulations. Still, they might be of interest, since they provide a more intuitive quantification of the well interaction with the fractures.

Table 1. Notation[a]

Symbol	Definition	Reference
A	Reservoir drainage area $[L^2]$	
A_j	Intersection of a mesh triangle with a control volume	equation (21c)
a_i	Areal coordinates in a triangle	equation (25)
b	Fracture aperture $[L]$	
C_A	Shape factor $[-]$	equation (34)
C_f	Total compressibility (fracture)	equation (6)
C_g	Total compressibility (homogeneous medium)	equation (43)
C_i	Coefficient of the discretized equations	equation (20)
C_m	Total compressibility (matrix)	equation (2)
$d^{\pm}$	Distance between mesh points on the well	equation (28a)
D_f	Pressure diffusivity (fracture)	equation (7)
$\tilde{D}_f$	Apparent pressure diffusivity	equation (22)
D_m	Pressure diffusivity (matrix)	equation (3)
D_s	Modified pressure diffusivity	equation (38)
$Ei(x)$	Exponential integral function	equation (32)
H	Fracture spacing	
h_p	Length of well segment in a control volume	equation (28a)
$\boldsymbol{I}$	Unit tensor	
$\mathcal{I}_{ij}$	Intersection line of fractures i and j	equation (8)
$\boldsymbol{j}$	Flow rate per unit width of a fracture	equation (4a)
J_0	Bessel function of zeroth order	equation (35)
$\boldsymbol{j}_i^{\pm}$	Flow rate in fracture i toward an intersection line	equation (8)
J_w	Flow rate per unit length from the well to the matrix $[L^2 T^{-1}]$	equation (2)
$J_{w,DA}$	Dimensionless flow rate J_w	equation (37c)
$J_{w,i}$	Flux from the well to a mesh point	equations (25) and (27)
K_a	Apparent permeability near the well	equation (46)
K_f	Fracture filling permeability	equation (5)
K_m	Matrix permeability $[L^2]$	
K_r	Apparent permeability relative to radial flow	equation (43)
K_w	Well hydraulic conductivity $[L^4]$	equation (10)
K_{eff}	Global effective permeability	
L	Sample size	
l	Length of well segment	section 3.2.3
M_{ij}	Coefficient of the discretized equations	equation (20)
$\boldsymbol{n}$	Normal vector to fracture plane	
N_{fr}	Number of fractures in a sample	Figure 1
N_I	Mean number of well/fracture intersections in the unit cell	equation (40)
n_I	Number of well/fracture intersections in the unit cell	equation (42)
$\boldsymbol{n}_\tau$	Unit vector normal to the domain boundary ∂_τ	equation (12b)
P	Pressure	
$p, p \pm 1$	Mesh points on the well	equation (28a)
$P^{\pm}$	Pressure on either sides of a fracture	Figure 2b
P_0	Initial pressure	equation (13)
P_f	Pressure in the fracture	Figure 2b
P_{s_h}	Well pressure	equation (11)
P_p	Pressure at a mesh point on the well	equation (28a)
P_w	Well pressure	equation (9)
P_∞	Far-field pressure	equation (12a)
$P_{0,DA}$	Intercept of pressure curve with ordinate axis	equation (44)
$P_{w,DA}$	Dimensionless pressure based on the drainage area	equation (37b)
$q^{\pm}$	Fracture/matrix exchanges	equation (21c)
Q_w	Total well flow rate $[L^3 T^{-1}]$	equation (9)
R	Characteristic fracture extent or radius	equation (15)
r	radial distance from the well	equation (23)
$\boldsymbol{r}$	Position vector	
r_a	Radius of damaged zone	equation (46)
r_w	Well radius	equation (10)
$\boldsymbol{r}_w$	Position vector of a mesh point on the well	section 3.2.3
$r_{w,a}$	Apparent well radius	equation (48)
S	Skin factor	equation (45)
s	Distance along the well from its head s_h	equation (9)
$\mathcal{S}$	Volumetric surface area of the fracture network	equation (39)
s_I	Well/fracture intersection spacing	equation (42)
S_I	Mean well/fracture intersection spacing	equation (41)
T, T_j	Triangular mesh element	
t	Time	
t_{DA}	Dimensionless time based on the drainage area	equation (37a)
$\boldsymbol{v}$	Seepage velocity in the matrix	equation (1)
$\boldsymbol{v}_\perp, \boldsymbol{v}^{\pm}$	Seepage velocity normal to a fracture	equations (4b) and (6)
v_i	Volume coordinates in a tetrahedron	equation (27)
V_{ex}	Excluded volume	section 6.1

Table 1. (continued)

Symbol	Definition	Reference
W	Productivity index	section 3.2.3
$\boldsymbol{x}_w$	Horizontal location of the well	Figure 3c
Y_0	Bessel function of zeroth order	equation (35)
β	Geometrical factor	equation (26)
$\gamma = 0.57722\ldots$	Euler's constant	equation (36)
$\delta(s)$, δ_w	Dirac functions	equations (9) and (2)
δ_M	Typical mesh point spacing	section 3.1
ΔP	Pressure drop across a fracture	equation (4b)
δt	Time step	section 3.3
ϵ_f	Porosity of fracture filling	equation (6)
ϵ_g	Porosity of an homogeneous medium	equation (43)
ϵ_m	Matrix porosity	equation (2)
η	Compressibility ratio	equation (15d)
μ	Fluid viscosity	
ν_{ij}	Vector normal to the intersection $\mathcal{I}_{ij}$	equation (8)
$\Pi_{w,\,DA}$	Log-time derivative of $P_{w,DA}$	section 5
Θ	Tetrahedral volume element	
ρ'	Fracture network density	section 6.1
ρ'_c	Critical fracture network density	section 6.1
σ	Fracture hydraulic conductivity $[L^3]$	equation (4a)
τ, $\partial\tau$	Sample volume, and its boundary	equation (12)
Ω, $\partial\Omega$	Control volume and its boundary	section 3.2
Ω_f, $\Omega^\pm$	Parts of Ω in the matrix and fracture	section 3.2.2
∇_s	Gradient operator restricted to a surface	equation (4a)

[a] Unlisted primed symbols are dimensionless parameters defined according to equation (15).

[116] First, an apparent well radius $r_{w,a}$ can be introduced as

$$r_{w,a} = r_w\, e^{-S} \qquad (48)$$

Equations (45) is then equivalent to equation (34) with r_w replaced by $r_{w,a}$. The apparent radius $r_{w,a}$ is plotted in Figure 9b. Of course, this semilogarithmic plot is equivalent to the linear plot of S in Figure 9a, and the fit (47) can be used in equation (48) for the estimation of $r_{w,a}$. However, the order of magnitude of $r_{w,a}$ is interesting. The apparent radius is larger than $r_w = R/100$ when the spacing s_I is smaller than about $3/2\ S_I$. It reaches about half the fracture radius for the spacings $s_I \sim S_I/2$, and it could even be larger for smaller spacings, although the probability of such an event is very small. On the opposite limit of large spacings, the apparent radius can be much smaller than r_w. Thus the fracturation of the matrix has two distinct effects. On one hand, it increases the medium permeability and the well efficiency. On the other hand, it also enhances the exchanges of the well with its surrounding, except when the well happens to be very poorly connected with the fracture network.

[117] Another interpretation of the parameter S as a skin factor can be given as follows. One may consider the fractured medium crossed by the well as an equivalent medium with permeability K_a. Note that K_a may differ from K_{eff}. For instance, for small densities $\rho' < \rho'_c$, the fractures are poorly connected which limits their influence on the permeability K_{eff}, whereas even isolated fractures fully contribute to enhance the transfers with the well. If we assume that K_a applies in a cylinder with radius R around the well, it is related to S by equation (46), which yields

$$K_a = \frac{1}{1 - \dfrac{S}{\ln r_w/R}} K_{eff} \qquad (49)$$

The results plotted in Figure 9c versus n_I/N_I show that for $\rho' \geq 4$, K_a increases roughly linearly with the density of intersections,

$$\frac{K_a}{K_{eff}} \approx 1.31 + 0.94\left(\frac{n_I}{N_I} - 1\right) \qquad (r = 0.89) \qquad (50)$$

However, the data for $\rho' = 1.48$ are very scattered, which means that for small fracture densities, the interaction of the well with the fractures cannot be modeled by such a simple model.

7.   Concluding Remarks

[118] The numerical model presented in this paper for 3-D single-phase compressible flow through fractured porous media was shown to perform well in simple reference cases and was applied to simulate well testing in randomly fractured media.

[119] The flexibility of the numerical description of the discrete fracture network makes it possible to directly simulate the operation of a well in a real setting, given field data relative to the fracture locations and characteristics. In addition, the fact that the numerical mesh is generated prior to the introduction of the well allows for an easy optimization of the well design, according to any relevant criterion.

[120] Although it was not illustrated in this paper, the numerical model is ready to handle heterogeneous matrix or fracture properties, far from or in the absence of the well. This is an important feature, in view of the experiments and simulations of *Sonnenborg et al.* [1999], which showed that spatial variations of the fracture aperture may have a significant influence on the exchanges with the matrix. Additional work is needed to accurately describe the fluid exchanges between a well and its heterogeneous surroundings.

[121] Another desirable extension of the model is the incorporation of two-phase flow, which will be addressed in the near future.

References

Acuna, J. A., and Y. C. Yortsos, Application of fractal geometry to the study of networks of fractures and their pressure transient, *Water Resour. Res.*, *31*, 527–540, 1995.

Adler, P. M., and J.-F. Thovert, *Fractures and Fracture Networks*, Kluwer Acad., Norwell, Mass., 1999.

Banerjee, R., D. Gunasekera, and K. J. Clark Fletcher, Simulation of hydraulically fractured horizontal and vertical wells to well testing: Accuracy using unstructured grids, in *Proceedings of the 7th European Conference on the Mathematics of Oil Recovery, ECMOR, Baveno, Italy*, paper M21, Eur. Assoc. of Geosci. and Eng., Houten, Netherlands, 2000.

Barenblatt, G. I., and Yu. P. Zheltov, Fundamental equations of filtration of homogeneous liquids in fissured rocks, *Dokl. Akad. Nauk SSSR*, *13*, 545–548, 1960.

Bogdanov, I. I., V. V. Mourzenko, J.-F. Thovert, and P. M. Adler, Effective permeability of fractured porous media in steady-state flow, *Water Resour. Res.*, *107*, doi:10.1029/2001WR000756, in press, 2002.

Boulton, N. S., and T. D. Streltsova, Unsteady flow to a pumped well in a two-layered water-bearing formation, *J. Hydrol.*, *35*, 245–256, 1977a.

Boulton, N. S., and T. D. Streltsova, Unsteady flow to a pumped well in a fissured water-bearing formation, *J. Hydrol.*, *35*, 257–270, 1977b.

Bourdarot, G., *Essais de Puits: Méthodes d'Interprétation*, Technip, Paris, 1996.

Carslaw, H. S., and J. C. Jaeger, *Conduction of Heat in Solids*, 2nd ed., 510 pp., Clarendon, Oxford, England, 1959.

Chen, Z.-X., Transport flow of slightly compressible fluids through double-porosity, double-permeability systems: A state-of-the-art review, *Transp. Porous Media*, *4*, 97–116, 1989.

Durlofsky, J. F., An approximate model for well productivity in heterogeneous porous media, *Math. Geol.*, *32*, 421–438, 2000.

Earlougher, R. C., *Advances in Well Test Analysis*, Soc. Pet. Eng. AIME Monogr. Ser., vol. 5, Henry L. Doherty Mem. Fund of AIME, New York, 1977.

Gradshteyn, I. S., and I. M. Ryshik, *Tables of Integrals, Series and Products*, Academic, San Diego, Calif., 1965.

Gringarten, A. C., and H. J. N. Ramey, Unsteady-state pressure distributions created by a well with a single horizontal fracture, partial penetration, or restricted entry, *Soc. Pet. Eng. J.*, *14*, 413–426, 1974.

Gringarten, A. C., H. J. Ramey, and R. Raghavan, Unsteady-state pressure distributions created by a well with a single infinite conductivity vertical fracture, *Soc. Pet. Eng. J.*, *14*, 347–360, 1974.

Gwo, J. P., R. O'Brien, and P. M. Jardine, Mass transfer in structured porous media: Embedding mesoscale structure and microscale hydrodynamics in a two-region model, *J. Hydrol.*, *208*, 204–222, 1998.

Huseby, O., J.-F. Thovert, and P. M. Adler, Geometry and topology of fracture systems, *J. Phys. A Math Gen.*, *30*, 1415–1444, 1997.

Huyakorn, P. S., and G. F. Pinder, *Computational Methods in Subsurface Flow*, Academic, San Diego, Calif., 1983.

Koudina, N., R. Gonzalez-Garcia, J.-F. Thovert, and P. M. Adler, Permeability of three-dimensional fracture networks, *Phys. Rev. E*, *57*, 4466–4479, 1998.

Mo, H. H., M. Bai, D. Z. Lin, and J.-C. Roegiers, Study of flow and transport in fracture network using percolation theory, *Appl. Math. Modelling*, *22*, 277–291, 1998.

Noetinger, B., and T. Estebenet, Up-scaling of double porosity fractured media using continuous-time random walks methods, *Transp. Porous Media*, *39*, 315–337, 2000.

Onur, M., and A. Satman, Interpretation of single-well pressure transient data from naturally fractured reservoirs, *In Situ*, *22*, 181–237, 1998.

Reis, J. C., Effect of fracture spacing distribution on pressure transient response in naturally fractured reservoirs, *J. Pet. Sci. Eng.*, *20*, 31–47, 1998.

Shikaze, S. G., E. A. Sudicky, and F. W. Schwartz, Density dependent solute transport in discretely-fractured geological media: Is prediction possible?, *J. Contam. Hydrol.*, *34*, 273–291, 1998.

Snow, D. T., Anisotropic permeability of fractured media, *Water Resour. Res.*, *5*, 1273–1289, 1969.

Sonnenborg, T. O., M. B. Butts, and K. H. Jensen, Aqueous flow and transport in analog systems of fractures embedded in permeable matrix, *Water Resour. Res.*, *35*, 719–729, 1999.

Streltsova, T. D., *Well Testing in Heterogeneous Formations*, John Wiley, New York, 1988.

Sudicky, E. A., A. J. A. Unger, and S. Lacombe, A noniterative technique for the direct implementation of well bore boundary conditions in three-dimensional heterogeneous formations, *Water Resour. Res.*, *31*, 411–415, 1995.

Warren, J. R., and P. J. Root, The behaviour of naturally fractured reservoirs, *Soc. Pet. Eng. J.*, *228*, 245–255, 1963.

Weir, G. J., Single-phase flow regimes in a discrete fracture model, *Water Resour. Res.*, *35*, 65–73, 1999.

Wilson, C. R., and P. A. Witherspoon, Steady state flow in rigid networks of fractures, *Water Resour. Res.*, *10*, 328–335, 1974.

Young, R., Pressure transient in a double-porosity medium, *Water Resour. Res.*, *28*, 1261–1270, 1992.

———————————

P. M. Adler, Institut de Physique du Globe de Paris, tour 24, 4 Place Jussieu, 75252 Paris Cedex 05, France. (adler@ipgp.jussieu.fr)

I. I. Bogdanov, V. V. Mourzenko, and J.-F. Thovert, Laboratoire de Combustion et de Detonique, SP2MI, BP 179, 86960 Futuroscope Cedex, France.